

# Identifying Drift, Diffusion, and Causal Structure from Temporal Snapshots

**Vincent Guan**

*Department of Mathematics*

*University of British Columbia, Vancouver, Canada*

VGUAN23@MATH.UBC.CA

**Joseph Janssen**

*Department of Earth, Ocean and Atmospheric Sciences*

*University of British Columbia, Vancouver, Canada*

JOEJANSSEN@EOAS.UBC.CA

**Hossein Rahmani**

*Department of Mathematics*

*University of British Columbia, Vancouver, Canada*

RAHMANI.HOSSEIN1380@GMAIL.COM

**Andrew Warren**

*Department of Mathematics*

*University of British Columbia, Vancouver, Canada*

AWARREN@MATH.UBC.CA

**Stephen Y. Zhang**

*School of Mathematics and Statistics*

*University of Melbourne, Melbourne, Australia*

SYZ@SYZ.ID.AU

**Elina Robeva**

*Department of Mathematics*

*University of British Columbia, Vancouver, Canada*

EROBEVA@MATH.UBC.CA

**Geoffrey Schiebinger**

*Department of Mathematics*

*University of British Columbia, Vancouver, Canada*

GEOFF@MATH.UBC.CA

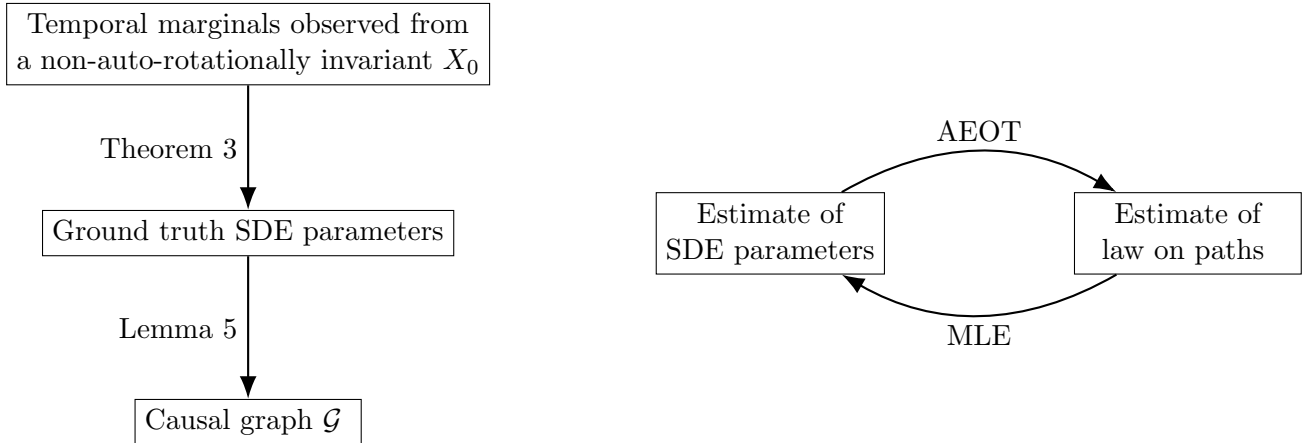
## Abstract

Stochastic differential equations (SDEs) are a fundamental tool for modelling dynamic processes, including gene regulatory networks (GRNs), contaminant transport, financial markets, and image generation. However, learning the underlying SDE from data is a challenging task, especially if individual trajectories are not observable. Motivated by burgeoning research in single-cell datasets, we present the first comprehensive approach for jointly identifying the drift and diffusion of an SDE from its temporal marginals. Assuming linear drift and additive diffusion, we prove that these parameters are identifiable from marginals if and only if the initial distribution lacks any generalized rotational symmetries. We further prove that the causal graph of any SDE with additive diffusion can be recovered from the SDE parameters. To complement this theory, we adapt entropy-regularized optimal transport to handle anisotropic diffusion, and introduce APPEX (Alternating Projection Parameter Estimation from  $X_0$ ), an iterative algorithm designed to estimate the drift, diffusion, and causal graph of an additive noise SDE, solely from temporal marginals. We show that APPEX iteratively decreases Kullback–Leibler divergence to the true solution, and demonstrate its effectiveness on simulated data from linear additive noise SDEs.

**Keywords:** Stochastic differential equations (SDEs), optimal transport, trajectory inference, causal inference, Schrodinger Bridge

## 1 Introduction

This work presents the first comprehensive approach for jointly identifying the drift and diffusion of a stochastic differential equation (SDE) from observed temporal marginals. While parameter estimation has been studied extensively using trajectory data, either from one long trajectory (Nielsen et al., 2000; Bishwal, 2007), or multiple short trajectories (Manten et al., 2024; Lu et al., 2021;



(a) Theoretical contributions: identifying drift, diffusion, and causal structure from temporal marginals

(b) Algorithmic contributions: APPEX algorithm

Figure 1: Outline of our theoretical (a) and algorithmic (b) contributions. In (b), our algorithm Alternating Projection Parameter Estimation from  $X_0$  alternates between Anisotropic Entropy-regularized Optimal Transport (AEOT) and Maximum Likelihood Estimation (MLE).

Pawlowicz et al., 2019), it is often impossible to observe individual trajectories when tracking large populations. For example, in single-cell RNA sequencing (scRNA-seq) datasets, the destructive nature of sequencing technologies prevents specific cells from being tracked over time (Trapnell et al., 2014; Setty et al., 2016; Farrell et al., 2018). Similarly, hydrogeochemical sensors cannot track distinct particles when studying contaminant flow, providing only data on plume migration (Man and Tsai, 2007; Hazas et al., 2023; Salamon et al., 2007; Elfeki, 2006; Adams and Gelhar, 1992; Boggs et al., 1992; Mackay et al., 1986; Nenna et al., 2011). Observational data may therefore be limited to samples from temporal marginals of the process at various measurement times. We refer to this observational setting as *marginals-only*.

However, many stochastic processes are non-identifiable under the marginals-only setting, since their distributions may evolve identically, despite having distinct individual trajectories (Weinreb et al., 2018). Previous works therefore simplify the problem, by assuming that the drift is irrotational and that the diffusion is isotropic, with known diffusivity (Weinreb et al., 2018; Lavenant et al., 2021; Vargas et al., 2021; Chizat et al., 2022).

## 1.1 Our contributions

We prove that for a large class of initial distributions, the drift, diffusion, and underlying causal graph of an SDE with linear drift and additive diffusion can be identified from its temporal marginals. We also introduce a practical algorithm for estimating each of these quantities solely from the marginals of a general additive diffusion process, and demonstrate the effectiveness of our method on simulated data. We illustrate our theoretical contributions in Figure 1a and our algorithmic contributions in Figure 1b. A detailed overview of our contributions is also given below.

1. We provide a theoretical foundation for system identification from temporal marginals in Section 3.
  - (a) In Theorem 3, we fully characterize the conditions for guaranteeing identifiability of linear drift and additive diffusion from observed marginals. Identifiability is guaranteed if and only if the initial distribution  $X_0$  is not auto-rotationally invariant (Definition 2).

- (b) In Lemma 5, we connect parameter estimation to causal structure learning via dynamic structural causal models (Boeken and Mooij, 2024). We show that the causal graph of any additive noise model can be recovered from the SDE parameters.
- 2. In Section 4, we introduce our algorithm: Alternating Projection Parameter Estimation from  $X_0$  (APPEX). It is the first method designed to estimate drift and diffusion from temporal marginals of additive noise SDEs, without prior knowledge.
  - (a) We show that with each iteration, APPEX’s estimates approach the true solution. APPEX alternates between a trajectory inference step, which is a Schrödinger bridge problem, and a parameter estimation step, which is solved via maximum likelihood estimation.
  - (b) To solve the Schrödinger bridge problem for trajectory inference, we adapt entropic optimal transport for parameter dependent transport costs, including arbitrary anisotropic diffusion.
  - (c) We test APPEX’s efficacy across a wide range of experiments in Section 5. We first use APPEX to empirically demonstrate that classical non-identifiable linear additive noise SDEs are resolved when  $X_0$  is initialized appropriately according to Theorem 3. We then demonstrate APPEX’s effectiveness over a large-scale experiment on higher dimensional SDEs with randomly generated parameter sets. Our results demonstrate that APPEX identifies arbitrary linear additive noise SDEs with significantly higher accuracy than the widely-used Waddington-OT (WOT) method (Schiebinger et al., 2019). Our final experiments demonstrate that APPEX can be used to identify the system’s causal graph, even in the presence of correlated diffusion from latent confounders.

## 2 Background and related work

In this section, we first give an overview of SDEs and a discussion of some real-world applications. We then review relevant literature and techniques for statistical inference from the “marginals-only” observational setting. Finally, we discuss the problem of non-identifiability of SDEs under this setting.

### 2.1 Stochastic differential equations (SDEs) and modeling real-world systems

The mathematical framework of SDEs, or drift-diffusion processes, originates from statistical mechanics. The drift models the velocity of particles flowing in a carrier fluid, while diffusion is driven by Brownian motion, and governs their dispersion due to random collisions (Einstein, 1956; MacInnes and Bracco, 1992). Formally, a  $d$ -dimensional time-homogeneous SDE is driven by an  $m$ -dimensional Brownian motion  $W_t$ , and is parameterized by a drift function  $b(x) : \mathbb{R}^d \rightarrow \mathbb{R}^d$  and a diffusion function  $\sigma(x) : \mathbb{R}^d \rightarrow \mathbb{R}^{d \times m}$ , such that

$$dX_t = b(X_t) dt + \sigma(X_t) dW_t, \quad X_0 \sim p_0, \quad (1)$$

where  $b(x)$  and  $\sigma(x)$  are Lipschitz to ensure the solution’s existence and uniqueness (Fang and Giles, 2020).

By capturing deterministic and stochastic dynamics, SDEs provide a powerful framework for modeling complex systems across a variety of fields. For example, SDEs have been used to model cell differentiation in single-cell biology, where a stem cell changes into another cell type, such as a blood cell or bone cell. The drift can be related to the set of genes that directly regulate the expression of a gene of interest (Zhang, 2024; Aalto et al., 2020; Atanackovic et al., 2024; Zhao et al., 2024; Tejada-Lapuerta et al., 2023), and therefore provides insights into genetic diseases and

gene therapies. Meanwhile, the diffusion informs the extent to which cell fates are determined by initial conditions (Forrow, 2024). In hydrological systems, drift is linked to important and unknown properties of the subsurface, such as hydraulic conductivity through average flow velocity (Hazaras et al., 2023; Beven et al., 1993), while the diffusion usually describes material heterogeneity or turbulence (Beven et al., 1993), and therefore informs the applicability of popular models, such as Darcy's law (Man and Tsai, 2007; Oh and Tsai, 2010; Lichtner et al., 2002). Together, these parameters determine pollutant fates in hydrological systems, a key concern in safeguarding drinking water sources (O'Connor et al., 2002; Frind et al., 2006; Locatelli et al., 2019; Chen et al., 1999; Paulson, 1997; Cahill et al., 2019). In addition to applications to physical sciences, SDEs have also been prominently used for pricing stocks and options in financial markets (Black and Scholes, 1973) and for image generation in computer vision (Meng et al., 2021).

In this paper, we consider time-homogeneous additive noise SDEs. These SDEs are characterized by an arbitrary drift function  $b(X_t)$  and a possibly anisotropic space-independent diffusion  $G \in \mathbb{R}^{d \times m}$ , such that

$$dX_t = b(X_t) dt + G dW_t, \quad X_0 \sim p_0. \quad (2)$$

We also refer to  $H = GG^\top \in \mathbb{R}^{d \times d}$  as the (observational) diffusion, since it is only possible to observe  $H$  (Wang et al., 2024; Pavliotis, 2014). Time-homogeneous linear additive noise SDEs are of particular interest (du Buisson and Touchette, 2023; Wang et al., 2024; Zhang, 2024), as they generalize the popular Ornstein-Uhlenbeck process by removing the assumption of stationarity. A time-homogeneous linear additive noise SDE obeys the form

$$dX_t = AX_t dt + G dW_t, \quad X_0 \sim p_0, \quad A \in \mathbb{R}^{d \times d}. \quad (3)$$

We overview important properties of this SDE in Section A.1 of the appendix, including its closed form solution and transition density.

## 2.2 Inference from temporal marginals

The marginals-only observational setting dates back to at least Aristotle, who dissected bird eggs at various developmental stages, in order to infer the processes and mediators (e.g., heat) behind embryogenesis (Waddington, 1935; Ogle et al., 1882; Aristotle, 1942). If the underlying system is modeled by an SDE, then the evolution of its temporal marginals  $p_t$  are defined by its Fokker-Planck equation. For example, a straightforward computation shows that the marginals of a linear additive noise SDE evolve according to the following Fokker-Planck equation:

$$\frac{\partial}{\partial t} p(x, t) = -\nabla \cdot ((Ax)p(x, t)) + \frac{1}{2} \nabla \cdot (H \nabla p(x, t)), \quad p(x, 0) = p_0(x). \quad (4)$$

Contemporary research in statistical inference from temporal marginals largely comes from single-cell biology. Many works focus on trajectory inference for cell fates (Schiebinger et al., 2019; Lavenant et al., 2021; Yachimura et al., 2023; Chizat et al., 2022), while others infer the causal graph, e.g. GRN (Aalto et al., 2020; Brouillard et al., 2020; Tejada-Lapuerta et al., 2023; Rohbeck et al., 2024), or perform parameter estimation (Chakraborty et al., 2009; Shen et al., 2024a). Recent works jointly estimate a subset of these quantities by leveraging their intrinsic relationships. For instance, Vargas et al. (2021) and Shen et al. (2024b) are primarily interested in trajectory inference, and iteratively estimate drift and trajectories. Meanwhile, Zhang (2024) iteratively estimates drift and trajectories, while additionally applying permanent interventions on the drift dynamics for network inference.

## 2.3 Schrödinger bridge problem

Given a set of temporal marginals, trajectory inference is the task of estimating a law on paths that obeys each marginal constraint while closely approximating desired reference dynamics. This

is commonly implemented by solving the Schrödinger Bridge (SB) problem (Chizat et al., 2022; Shen et al., 2024a), defined below for a pair of marginals. Given the transition law  $\mathcal{K}$  of a reference process, an initial distribution  $\mu$ , and a final distribution  $\nu$ , the SB solution is the law of the stochastic process, which satisfies both marginal constraints, while minimizing relative entropy to  $\mathcal{K}$ :

$$\pi^* = \text{Proj}_{\Pi(\mu, \nu)}^{KL}(\mathcal{K}) = \arg \min_{\pi \in \Pi(\mu, \nu)} D_{KL}(\pi \| \mathcal{K}). \quad (5)$$

The SB problem has also gained interest in the machine learning community, due to its connection to generative diffusion models. Score estimation of time-reversed SDEs is an instance of the SB problem (De Bortoli et al., 2021), and SB solvers are now widely used in generative modeling due to their flexibility (De Bortoli et al., 2021; Chen et al., 2021; Shi et al., 2024; Huang, 2024).

## 2.4 Identifiability of SDE parameters

The problem of non-identifiability occurs if there exists an alternative drift-diffusion pair, e.g.  $(\tilde{A}, \tilde{H}) \neq (A, H)$  for linear-additive noise SDEs, which shares the same marginals. Equivalently, the processes satisfy the same Fokker-Planck equation across all observed times, given initial distribution  $p_0$ . Non-identifiability can occur due to many factors. For example, distinct SDEs can share the same stationary distribution, and would hence be non-identifiable from marginals if  $p_0$  is initialized at equilibrium (Lavenant et al., 2021; Shen et al., 2024a). Also, if the initial distribution is standard normal  $p_0 \sim \mathcal{N}(0, I_d)$ , then it would be impossible to distinguish between a pure Brownian motion, and an SDE with an additional rotational vector field (Shen et al., 2024a). We overview three classical examples of non-identifiability in Section A of the Appendix.

Because of non-identifiability, previous works require assumptions about the underlying SDE to perform inference. The standard assumptions are that the drift is an irrotational vector field  $\nabla\psi$  (Weinreb et al., 2018; Lavenant et al., 2021; Vargas et al., 2021; Chizat et al., 2022; Terpin et al., 2024) and that the diffusion is both known and given by isotropic Brownian motion  $\sigma dW_t$  (Weinreb et al., 2018; Lavenant et al., 2021; Vargas et al., 2021; Chizat et al., 2022; Shen et al., 2024b; Zhang, 2024; Terpin et al., 2024). It is also common to leverage additional perturbational data from interventions, and to impose regularization, to better learn the system (Rohbeck et al., 2024; Zhang, 2024; Maddu et al., 2024). However, these constraints impose unrealistic conditions on the data. An irrotational drift field cannot model negative feedback loops or repressilator dynamics, which are common in biological data (Weinreb et al., 2018). Similarly, isotropic diffusion cannot model variable noise scales or correlated noise structures, which commonly arise in real data (Mogensen and Hansen, 2022; Rohbeck et al., 2024; Santos et al., 2024). While most works use a known diffusion estimate to infer drift, Forrow (2024) infers diffusion, but requires a drift estimate. In both cases, the accuracy of the prior estimate is crucial, because misspecified diffusion typically leads to poor drift estimation and vice-versa (Beven et al., 1993). This is problematic, since knowing drift or diffusion *a priori* is unrealistic in practice. Finally, we note that concurrent work estimates drift and diffusion, but does not consider the uniqueness of learned parameters, due to non-identifiability (Terpin et al., 2024; Brogat-Motte et al., 2024).

To advance the field of statistical inference from temporal marginals, we work to remove previous assumptions by determining conditions for identifiability and designing a method that leverages them. Wang et al. (2024) showed that identifiability of a linear additive noise SDE from ground truth trajectories with fixed  $X_0 \in \mathbb{R}^d$  is equivalent to a non-degenerate rank condition based jointly on  $X_0$ , the linear drift  $A$  and the observational diffusion  $GG^\top$ . In contrast, our work studies identifiability of linear additive noise SDEs in the more general “marginals-only” setting. We also demonstrate that identifiability is guaranteed across all linear additive noise SDEs solely from the properties of the initial distribution. To the best of our knowledge, this has not been shown even in the case of trajectory-based observations.

### 3 System identification from temporal marginals

We present our main theorem in Section 3.1. We prove that generalized rotational symmetries in the initial distribution  $X_0$  provide necessary and sufficient conditions for identifying the drift and diffusion parameters of linear additive noise SDEs from its time marginals. We then show that the underlying causal graph of a general additive noise SDE can be recovered from its drift and diffusion parameters in Section 3.2.

We first define the desired rotational properties. Recall that classical rotations in  $\mathbb{R}^d$  for  $d \geq 2$  are given by matrix exponentials  $e^{At}$ , such that  $t$  is the rotation angle and  $A$  is skew-symmetric, i.e.  $A + A^\top = 0$ . We may similarly define rotations over anisotropic geometries.

**Definition 1** *Let  $d \geq 2$ . We define a  $\Sigma$ -generalized rotation in  $\mathbb{R}^d$  as a matrix exponential  $e^{At}$ , such that  $t$  is the rotation angle and  $A \in \mathbb{R}^{d \times d}$  is skew-symmetric with respect to  $\Sigma \succeq 0$ , i.e.  $A\Sigma + \Sigma A^\top = 0$ .*

If  $\Sigma \succ 0$ , then  $\Sigma$ -generalized rotations are equivalent to classical rotations in a transformed space, such that lengths and angles are modified by scaling and shearing (see Lemma 10 in appendix). Intuitively, ellipsoids, defined by  $E_\Sigma = \{x \in \mathbb{R}^d : x^\top \Sigma^{-1} x = 1\}$ , are invariant under  $\Sigma$ -generalized rotations, since  $e^{At} E_\Sigma = E_\Sigma$ . We may similarly extend this definition for random variables.

**Definition 2** *Let  $X$  be a  $d$ -dimensional r.v. with covariance  $\Sigma$ .  $X$  is auto-rotationally invariant*

- if there exists a nontrivial  $\Sigma$ -generalized rotation  $e^{At}$  with  $A \neq 0$  such  $e^{At}X \sim X \forall t \geq 0$ , or
- if there exists an orthogonal transformation  $P$ , such that at least one component of  $P^\top X$  is mean 0 univariate Gaussian, i.e.  $(P^\top X)_1 \sim \mathcal{N}(0, \sigma^2)$ .

Conversely,  $X$  is not auto-rotationally invariant, if  $e^{At}X \sim X \forall t \geq 0$  admits only the solution  $A = 0$ , and none of its cross sections are univariate Gaussian.

Auto-rotational invariance is reminiscent of Maxwell's theorem, which states that if a random vector  $X$  has independent components, and is invariant to all classical rotations, then  $X \sim \mathcal{N}(0, \sigma^2 I_d)$  (Maxwell, 1860). Indeed, all mean 0 isotropic Gaussians are auto-rotationally invariant, since they are invariant under  $e^{At}$ , for any skew-symmetric  $A$ . To extend our definition to one dimensional subspaces, where rotations are undefined, we define mean 0 Gaussians as the only univariate auto-rotationally invariant distributions by convention.

However, auto-rotational invariance generalizes Maxwell's characterization in a few important ways. First, auto-rotational invariance generalizes rotations for anisotropic geometries defined by the covariance  $\Sigma$ , e.g.  $N(0, \Sigma)$  is auto-rotationally invariant (see Lemma 11 in appendix). Second, auto-rotational invariance only requires that there exists one matrix  $A$  such that  $e^{At}X \sim X$ , rather than invariance to all rotations, e.g. a stack of Gaussians  $X = \text{Unif}(-1, 1) \times N(0, \Sigma)$  would be auto-rotationally invariant. Furthermore, auto-rotational invariance does not assume independent components, and therefore permits any rotationally symmetric distribution (after shearing and scaling  $\mathbb{R}^d$  accordingly), e.g. uniform distributions over ellipsoids and cylindrical distributions are auto-rotationally invariant. Finally, the matrix  $A$  is not required to be related to a rotation, even after shearing and scaling the space. Indeed, all degenerate r.v.'s are auto-rotationally invariant, since  $e^{At}X \sim X$  would hold if  $X$  is in the nullspace of  $A$  with probability 1. It turns out that if  $X$  is non-degenerate and satisfies  $e^{At}X \sim X$  for some  $A \neq 0$ , then  $X$  has a density whose level sets are ellipsoids (see Lemma 12 in the appendix). Thus, almost all r.v.s are not auto-rotationally invariant. Figure 2 illustrates examples of auto-rotationally invariant r.v.s and Figure 8 in the appendix shows that there are only three types of auto-rotational invariance: rank-degenerate r.v.s, r.v.s that are invariant to a non-degenerate  $\Sigma$ -generalized rotation, and r.v.s containing a Gaussian cross-section.

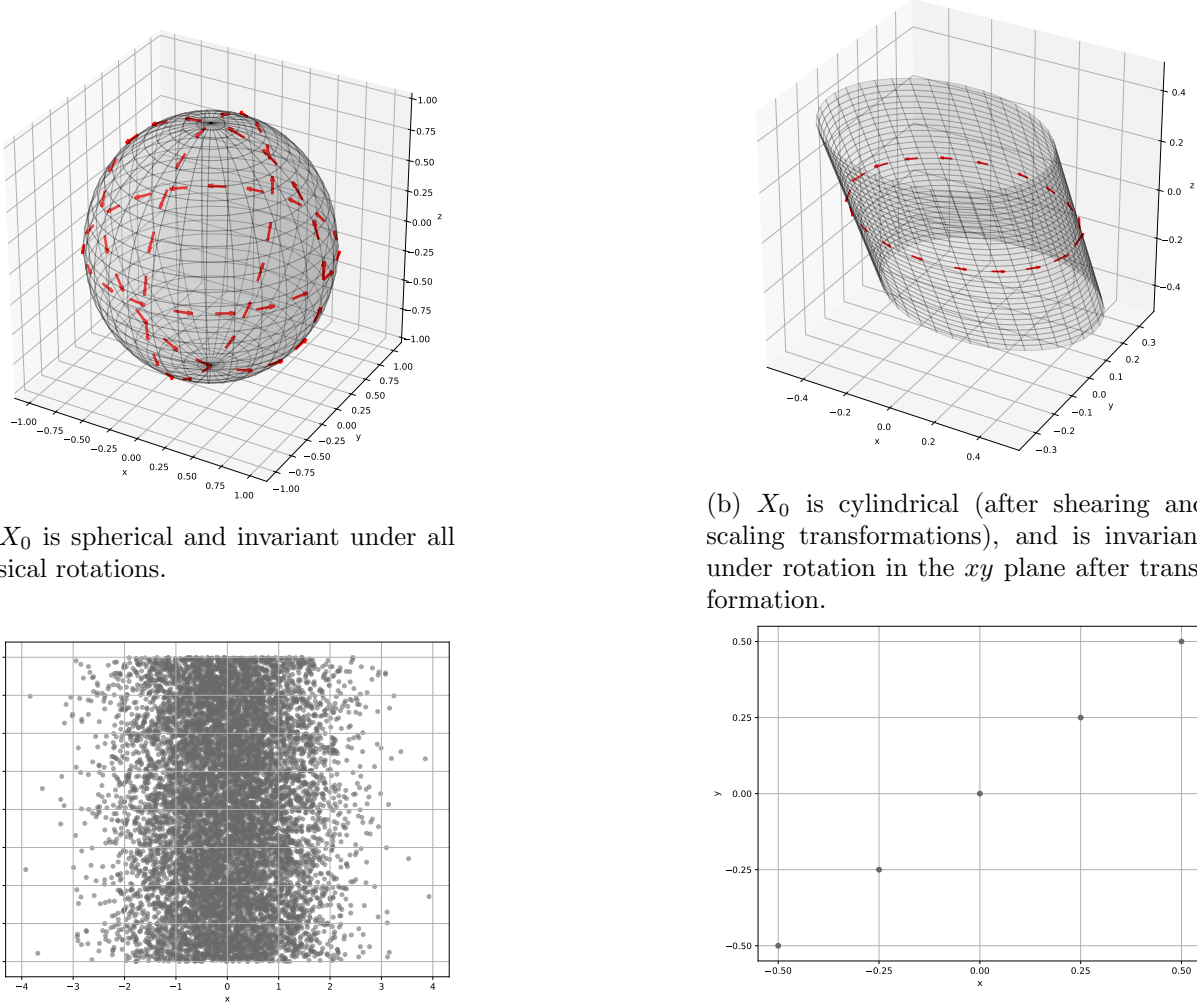


Figure 2: Four examples of auto-rotationally invariant distributions are illustrated. By Theorem 3, these initial distributions lead to non-identifiability of linear additive noise SDEs from temporal marginals.

### 3.1 SDE parameter identifiability

We are now ready for our main identifiability theorem, which characterizes identifiability of linear additive noise SDEs based on the auto-rotational invariance of the initial distribution  $X_0$ .

**Theorem 3** *Let  $p_0$  be a probability distribution on  $\mathbb{R}^d$  with finite moments, and let*

$$\Theta = \{(A, H) : A \in \mathbb{R}^{d \times d}, G \in \mathbb{R}^{d \times m}, H = GG^\top\}$$

*denote the set of drift-diffusion pairs under a linear additive noise model (3). Then, given the initialization  $X_0 \sim p_0$ , any parameter set  $(A, H) \in \Theta$  is identifiable from its marginals  $\{p_t : t \geq 0\}_{A, H}$ , in the sense that*

$$\text{if } \{p_t : t \geq 0\}_{A, H} = \{p_t : t \geq 0\}_{\tilde{A}, \tilde{H}} \text{ then } (A, H) = (\tilde{A}, \tilde{H}),$$

if and only if  $p_0$  is not auto-rotationally invariant.

In other words, identifiability of  $(A, H)$  from marginals is guaranteed if  $p_0$  is not auto-rotationally invariant. However, if  $p_0$  is auto-rotationally invariant, then there exist multiple drift-diffusion pairs  $(A, H) \in \Theta$  that would obey the same marginals from  $p_0$ .

**Proof** We first show that if  $X_0$  is auto-rotationally invariant, then there exist multiple systems with equivalent marginals for each time, but distinct parameter sets  $(A, H = GG^\top) \neq (\tilde{A}, \tilde{H} = \tilde{G}\tilde{G}^\top)$ . Since  $X_0$  is auto-rotationally invariant, then there exists a matrix  $A \neq 0$  such that  $e^{At}X_0 \sim X_0$ , or there exists a cross-section that is univariate Gaussian, i.e.  $(P^\top X_0)_1 \sim \mathcal{N}(0, \sigma^2)$  such that  $P^\top = P^{-1}$ .

If there is  $A \neq 0$  such that  $e^{At}X_0 \sim X_0$ , then distinguishing the presence of  $A$  in the linear drift would be impossible, provided that  $A$  is also skew-symmetric with respect to the diffusion  $H = GG^\top$ . Indeed, given that  $e^{At}X_0 \sim X_0$  and  $AH + HA^\top = 0$ , the following two processes would obey  $X_t \sim Y_t \forall t \geq 0, \gamma \in \mathbb{R}$ :

$$dX_t = \gamma G dW_t \quad X_0 \sim p_0 \quad (6)$$

$$dY_t = AY_t dt + \gamma G dW_t \quad Y_0 \sim p_0 \quad (7)$$

Intuitively,  $A$  induces a  $\Sigma$ -generalized rotation that is non-identifiable from  $X_0$ , where  $\Sigma = \text{Cov}(X_0)$ . The full proof for the distributional equivalence of (6) and (7) is given in the Appendix (Prop. 17).

Alternatively, suppose that  $(P^\top X_0)_1 \sim \mathcal{N}(0, \sigma^2)$ . Recall that  $\mathcal{N}(0, \sigma^2)$  is the stationary distribution of any one-dimensional OU process with drift:diffusivity ratio  $-1 : 2\sigma^2$  (Lavenant et al., 2021; Brogat-Motte et al., 2024). Thus, the SDEs

$$d(P^\top X_t) = \begin{bmatrix} -\frac{1}{2} & \mathbf{0} \\ \mathbf{0} & A_{2,2} \end{bmatrix} P^\top X_t dt + \begin{bmatrix} \sigma & \mathbf{0} \\ \mathbf{0} & G_{2,2} \end{bmatrix} dW_t \quad X_0 \sim p_0 \quad (8)$$

$$d(P^\top Y_t) = \begin{bmatrix} -\frac{\alpha^2}{2} & \mathbf{0} \\ \mathbf{0} & A_{2,2} \end{bmatrix} P^\top Y_t dt + \begin{bmatrix} \alpha\sigma & \mathbf{0} \\ \mathbf{0} & G_{2,2} \end{bmatrix} dW_t \quad Y_0 \sim p_0. \quad (9)$$

would obey the same marginals  $P^\top X_t \sim P^\top Y_t$  for all  $t \geq 0$ . Both SDEs are distributionally identical in the first component, since they would stay at the stationary distribution  $\mathcal{N}(0, \sigma^2)$ . The SDEs also trivially obey the same law in the complementary subspace. It then follows that  $X_t \sim Y_t$  would hold  $\forall t \geq 0$  given the SDEs

$$dX_t = P \begin{bmatrix} -\frac{1}{2} & \mathbf{0} \\ \mathbf{0} & A_{2,2} \end{bmatrix} P^\top X_t dt + P \begin{bmatrix} \sigma & \mathbf{0} \\ \mathbf{0} & G_{2,2} \end{bmatrix} dW_t \quad X_0 \sim p_0 \quad (10)$$

$$dY_t = P \begin{bmatrix} -\frac{\alpha^2}{2} & \mathbf{0} \\ \mathbf{0} & A_{2,2} \end{bmatrix} P^\top Y_t dt + P \begin{bmatrix} \alpha\sigma & \mathbf{0} \\ \mathbf{0} & G_{2,2} \end{bmatrix} dW_t \quad Y_0 \sim p_0. \quad (11)$$

We now prove that identifiability is guaranteed if  $X_0$  is not auto-rotationally invariant. Suppose that  $X_t \sim Y_t$  for all  $t \geq 0$ , such that the first system has parameters  $(A, H = GG^\top)$  and the second system has parameters  $(\tilde{A}, \tilde{H} = \tilde{G}\tilde{G}^\top)$ . Recall that linear additive noise SDEs admit closed form solutions:

$$X_t = e^{At}X_0 + \int_0^t e^{A(t-s)}G dW_s$$

$$Y_t = e^{\tilde{A}t}X_0 + \int_0^t e^{\tilde{A}(t-s)}\tilde{G} dW_s,$$

such that  $e^{At}X_0 \perp \int_0^t e^{A(t-s)}GdW_s$  due to the independent increments of Brownian motion. Furthermore,

$$\begin{aligned} \int_0^t e^{A(t-s)}GdW_s &\sim \mathcal{N}(0, \Sigma_t) \text{ such that } \Sigma_t = \int_0^t e^{A(t-s)}He^{A^\top(t-s)}ds \text{ and} \\ \int_0^t e^{\tilde{A}(t-s)}\tilde{G}dW_s &\sim \mathcal{N}(0, \tilde{\Sigma}_t) \text{ such that } \tilde{\Sigma}_t = \int_0^t e^{\tilde{A}(t-s)}\tilde{H}e^{\tilde{A}^\top(t-s)}ds. \end{aligned}$$

Since  $X_t \sim Y_t$ , then the cumulant generating functions  $K_{X_t}(v) = \log(\mathbb{E}[e^{v^\top X_t}]) = K_{e^{At}X_0}(v) - \frac{1}{2}v^\top \Sigma_t v$  and  $K_{Y_t}(v) = \log(\mathbb{E}[e^{v^\top Y_t}]) = K_{e^{\tilde{A}t}X_0}(v) - \frac{1}{2}v^\top \tilde{\Sigma}_t v$  are equal for all  $t \geq 0$ . This gives us the equation

$$K_{X_0}(e^{A^\top t}v) - K_{X_0}(e^{\tilde{A}^\top t}v) = \frac{1}{2}v^\top (\Sigma_t - \tilde{\Sigma}_t)v \quad \forall t \geq 0. \quad (12)$$

We may rewrite the cumulant generating functions in terms of their power series expansions (McCULLAGH, 1984)

$$K_{X_0}(e^{A^\top t}v) = \sum_{n=0}^{\infty} \frac{1}{n!} T_n(e^{A^\top t}v, \dots, e^{A^\top t}v) \text{ and } K_{X_0}(e^{\tilde{A}^\top t}v) = \sum_{n=0}^{\infty} \frac{1}{n!} T_n(e^{\tilde{A}^\top t}v, \dots, e^{\tilde{A}^\top t}v),$$

where the tensor  $T_n$  is the symmetric tensor of order  $n$ , which defines the  $n$ th cumulant of  $X_0$ . To simplify the analysis, we perform the change of variables  $w(t) = e^{A^\top t}v$ ,  $v = e^{-A^\top t}w(t)$ . Let  $\bar{A} = \tilde{A}^\top - A^\top$ , and suppose for contradiction that  $\bar{A} \neq 0$ . Applying this change of variables to (12) yields

$$\begin{aligned} \sum_{n=0}^{\infty} \frac{1}{n!} &\left( T_n(w(t), \dots, w(t)) - T_n(e^{\bar{A}t}w(t), \dots, e^{\bar{A}t}w(t)) \right) \\ &= \frac{1}{2}w(t)^\top \left( \int_0^t e^{-As}He^{-A^\top s}ds - e^{\bar{A}^\top t} \int_0^t e^{-\bar{A}s}\tilde{H}e^{-\bar{A}^\top s}ds e^{\bar{A}t} \right) w(t). \end{aligned}$$

Since the RHS is purely quadratic in  $w(t)$ , it follows that for all  $n \geq 3$ , we have

$$T_n(w(t), \dots, w(t)) = T_n(e^{\bar{A}t}w(t), \dots, e^{\bar{A}t}w(t)) \quad (13)$$

In other words, for every choice of  $n$ -repeated arguments  $(w, \dots, w)$ , the value of  $T_n$  remains the same if we multiply each of the  $n$  components by  $e^{\bar{A}t}$ . Now, consider the Jordan form  $\bar{A} = P(D + N)P^{-1}$ , such that

$$e^{\bar{A}t} = Pe^{Dt}e^{Nt}P^{-1}$$

Then we may apply (13) on the repeated argument  $(Pw, \dots, Pw)$

$$T_n(Pw, \dots, Pw) = T_n(Pe^{Dt}e^{Nt}w, \dots, Pe^{Dt}e^{Nt}w)$$

However, we note that  $S_n(w, \dots, w) := T_n(Pw, \dots, Pw)$  represents the  $n$ th cumulant of the r.v.  $P^\top X_0$ . Hence,  $\forall t \geq 0$ , we have equality of the symmetric tensors

$$S_n(w, \dots, w) = S_n(e^{Dt}e^{Nt}w, \dots, e^{Dt}e^{Nt}w). \quad (14)$$

Now, we first suppose that the diagonal matrix  $D$  contains at least one nonzero eigenvalue  $\lambda_1$ . Then, applying (14) on the argument  $(\hat{i}, \dots, \hat{i})$ , where  $\hat{i}$  is the first canonical unit vector, yields

$$\begin{aligned} S_n(\hat{i}, \dots, \hat{i}) &= S_n(e^{Nt}\hat{i}, \dots, e^{Nt}\hat{i})e^{n\lambda_1 t} \\ &= S_n(\hat{i}, \dots, \hat{i})e^{n\lambda_1 t} \end{aligned}$$

where we have used multilinearity, and the fact that for any upper triangular Jordan block,  $N \cdot \hat{i} = 0$ . For this equality to hold  $\forall t \geq 0$ , we conclude that  $S_n(\hat{i}, \dots, \hat{i}) = 0$ , which implies that the  $n$ th cumulant of  $(P^\top X_0)_1$  is zero  $\forall n \geq 3$ . However, a classical result states that only Gaussian distributions have finitely many nonzero cumulants (Marcinkiewicz, 1939). Therefore, the first component of  $P^\top X_0$  is a univariate mean-0 Gaussian if  $\Sigma_t \neq \tilde{\Sigma}_t$ . This contradicts the fact that  $X_0$  is not auto-rotationally invariant. We also note that if  $\Sigma_t = \tilde{\Sigma}_t$ , then (12) implies that  $e^{\tilde{A}t} X_0 \sim X_0$ , since equality in all cumulants implies equality in distribution. This also contradicts the non-auto-rotational invariance of  $X_0$ , unless  $\tilde{A} = 0$ . Hence, we conclude that  $\tilde{A} = 0 \implies A = \tilde{A}$ . This trivially yields  $e^{At} X_0 \sim e^{\tilde{A}t} X_0$ , and forces the RHS of (12) to be 0, which in turn implies  $H = \tilde{H}$ , from the definition of  $\Sigma_t$  and  $\tilde{\Sigma}_t$ .

A similar argument holds in the case where all eigenvalues of  $D$  are zero, such that  $e^{Dt} e^{Nt} = e^{Nt}$ . Since  $N$  is an upper triangular Jordan block, we have for some  $k \in \mathbb{N}$  smaller than  $d$ ,

$$e^{Nt} = I + Nt + \frac{(Nt)^2}{2} + \dots + \frac{(Nt)^k}{k!} = \sum_{j=0}^k \frac{(Nt)^j}{j!},$$

In particular, all entries along the main diagonal of  $e^{Nt}$  are 1, i.e.  $(e^{Nt})_{i,i} = 1$ , and all entries along the super diagonal are  $t$ , i.e.  $(e^{Nt})_{i,i+1} = t$ . We may pick the vector  $v = [t \ 1 \ 0 \ \dots \ 0]^\top$  and easily check that

$$e^{Nt} v = \sum_{j=0}^k \frac{(Nt)^j}{j!} v = \begin{bmatrix} t+t \\ 1 \\ 0 \\ \vdots \\ 0 \end{bmatrix} = v + t\hat{i}$$

Therefore, applying (14) and multilinearity yields

$$\begin{aligned} S_n(v, \dots, v) &= S_n(v + t\hat{i}, \dots, v + t\hat{i}) \\ &= \sum_{k=0}^n \binom{n}{k} t^k S_n(\underbrace{v, \dots, v}_{n-k}, \underbrace{\hat{i}, \dots, \hat{i}}_k). \end{aligned}$$

Note that the  $k = 0$  term yields  $S_n(v, \dots, v)$ . We may rearrange and further apply multilinearity to yield:

$$0 = \sum_{k=1}^n \binom{n}{k} t^k S_n(\underbrace{v, \dots, v}_{n-k}, \underbrace{\hat{i}, \dots, \hat{i}}_k)$$

To satisfy this equation for all  $t$ , we must have  $S_n(\underbrace{\hat{j}, \dots, \hat{j}}_{n-k}, \underbrace{\hat{i}, \dots, \hat{i}}_k) = 0$  for all  $k = 1, \dots, n$ . The

case  $k = n$  implies that  $S_n(\hat{i}, \dots, \hat{i}) = 0$ . As argued in the previous case  $D \neq 0$ , this implies that  $(P^\top X_0)_1 \sim \mathcal{N}(0, \sigma^2)$ , or  $\Sigma_t = \tilde{\Sigma}_t$ . This yields identifiability  $A = \tilde{A}$  and  $H = \tilde{H}$  provided that  $X_0$  is not auto-rotationally invariant. ■

### 3.2 Causal graph identification from SDE parameters

Given that the drift and diffusion are identified, we can gain important insights into the system's causal structure. It has already been shown that knowing drift and diffusion provides the system's

post-intervention distributions (Hansen and Sokol, 2014; Wang et al., 2024). We prove under basic conditions that the causal graph  $\mathcal{G}$  of an additive noise SDE can be recovered from the drift  $b(X_t)$  and observational diffusion  $H = GG^\top$ .

Consider a  $d$ -dimensional additive noise SDE (2). By isolating the  $j$ th variable and integrating, we obtain:

$$X_t^{(j)} = X_0^{(j)} + \int_0^t b_j(X_s^{\alpha(j)}) \, ds + \sum_{k=1}^m G_{j,k} W_t^{(k)}, \quad (15)$$

where  $\alpha(j) \subset [d]$  is the set of variables that are used as input in  $b_j(X_t)$ . Then, (15) is an example of a dynamic structural causal model (Boeken and Mooij, 2024). In particular, we can define a causal graph  $\mathcal{G}$  over vertices  $V = [d]$  and edges  $E = \{i \rightarrow j : j \in [d], i \in \alpha(j)\}$  (Boeken and Mooij, 2024)[Definition 2]. Intuitively, given  $j \in V$ , we include the edge  $i \rightarrow j$  if  $X_t^{(i)}$  influences the evolution of  $X_t^{(j)}$  through the drift. Under an additive noise model, the diffusion  $\sigma(X_t) = G$  is space-independent, and does not contribute edges between vertices. However, if  $G$  is anisotropic, then the diffusion induces correlations between variables through shared driving noise (Santos et al., 2024). In this paper, we interpret shared driving noise as evidence of a latent confounder.

**Definition 4** Let  $X$  evolve according to a  $d$ -dimensional additive noise SDE:  $dX_t = b(X_t) \, dt + G \, dW_t$ . We define a multi-directed edge  $\tilde{e} = (i_1, \dots, i_p) \in \mathcal{G}$  if variables  $X^{(i_1)}, \dots, X^{(i_p)}$  depend on a common noise source  $W_t^{(k)}$ ,  $k \in [m]$ .

This definition follows standard convention in the static setting, where latent confounders introduce dependencies between noise terms in a functional causal model. In this framework, multidirected edges represent sets of variables whose noise terms are dependent due to a shared latent confounder (Liu et al., 2021). In the dynamic setting, shared driving noise has similarly been used to model latent confounders (see Lorch et al. (2024) and Boeken and Mooij (2024)[Example 4]). However, we note that this is not a comprehensive characterization of latent confounders in the dynamic setting, since confounding effects cannot always be attributed to diffusion. To address this, Mogensen and Hansen (2022) uses blunt edges to specifically denote correlated noise between two variables.

Under this causal framework, we show that the drift and diffusion identify all directed edges in the underlying causal graph, as well as all pairwise multidirected edges, i.e. bidirected edges.

**Lemma 5** Let  $X_t$  evolve according to a  $d$ -dimensional additive noise SDE:  $dX_t = b(X_t) \, dt + G \, dW_t$ , and let  $\mathcal{G} = (V = [d], E, \tilde{E})$  be its causal graph, over the variables  $X^{(1)}, \dots, X^{(d)}$ , with directed edge set  $E$  and multidirected edge set  $\tilde{E}$ .

- a. There exists a directed edge  $e = i \rightarrow j$  in  $\mathcal{G}$  if and only if  $b_j(X_t)$  depends on  $X_t^{(i)}$ .
- b. There exists a multidirected edge  $\tilde{e}$  containing  $(i, j)$  in  $\mathcal{G}$ , if and only if  $H_{i,j} = (GG^\top)_{i,j} \neq 0$ .

Thus,  $\mathcal{G}$  is identified by  $b(X_t)$  and  $H = GG^\top$  if no more than two variables share a common noise source.

**Proof** The first claim follows immediately from the definition of the dynamic structural causal model (15).

To prove the second claim, it is easy to see from (15) that  $X^{(i_1)}, \dots, X^{(i_p)}$  depends on a common noise source if and only if  $G_{i_1,k}, \dots, G_{i_p,k} \neq 0$  for some column  $k \in [m]$  in the diffusion  $G$ . Indeed, the existence of such a column implies that  $X^{(i_1)}, \dots, X^{(i_p)}$  each depend on  $W_t^{(k)}$ , and the other direction is given by the fact that  $W_t$  is a multivariate Gaussian process, with independent components. If two variables share a noise source, this condition is equivalent to  $H_{i,j} = G_i \cdot G_j \neq 0$ . We therefore conclude that there is a multidirected edge containing  $(i, j)$  in  $\mathcal{G}$  if and only if  $H_{i,j} \neq 0$ .

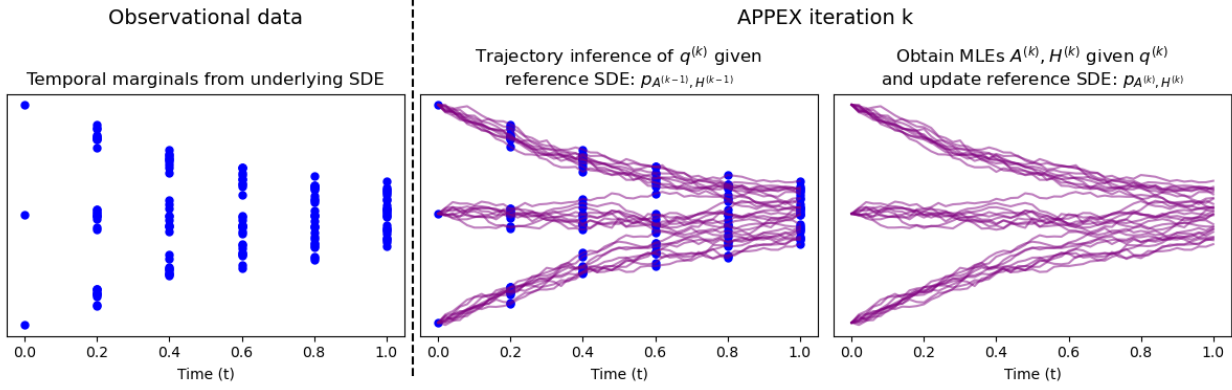


Figure 3: Visualization of our parameter estimation algorithm APPEX. Given observed temporal marginals from an underlying SDE (left), APPEX alternates between trajectory inference (middle) and MLE parameter estimation (right) in order to find the SDE parameters that best represent the temporal marginal observations.

■

Lemma 5 enables arbitrary causal structures to be learned from the drift, as well as pairwise shared noise structures from the diffusion. Combining Theorem 3 and Lemma 5 shows that we can identify the full causal structure of a linear additive noise SDE from its marginals if and only if  $X_0$  is non-auto-rotationally invariant. This result is particularly important for GRN inference, since our mathematical framework encompasses rotational drift, which can model feedback and repressor dynamics (Weinreb et al., 2018).

#### 4 Our parameter estimation method

In this section, we introduce our method, Alternating Projection Parameter Estimation from  $X_0$  (APPEX), which estimates a process' drift, diffusion, and causal graph from observed temporal marginals. Figure 3 illustrates the general strategy of the APPEX algorithm. We focus on linear additive noise SDEs, since Theorem 3 guarantees identifiability given that  $X_0$  is not auto-rotationally invariant. However, our algorithm can be used to estimate any additive noise SDE in the form of Equation 2. In this section, we give an intuitive explanation at the population level, using the process' true temporal marginals  $p_i \sim X_{t_i}$ . In Section 5, we perform experiments using empirical marginals  $\hat{p}_i$ , with finite samples per marginal.

Let  $p_0, \dots, p_{N-1}$  denote a set of observed temporal marginals, and let  $(A^{(0)}, H^{(0)})$  denote initial guesses for the drift and diffusion. The idea is to use an alternating optimization algorithm to obtain increasingly better estimates for the drift and diffusion matrices. Formally, we consider the spaces

$$\mathcal{D} = \{q : q_0 = p_0, \dots, q_{N-1} = p_{N-1}\} \text{ and} \quad (16)$$

$$\mathcal{A} = \left\{ p : \exists (A, H) \in \mathbb{R}^{d \times d} \times S_{\geq 0}^d \text{ s.t. } p(x, t + \Delta t \mid y, t) = \mathcal{N}\left(e^{A\Delta t}y, \int_0^{\Delta t} e^{As} H e^{A^\top s} ds\right) \right\}. \quad (17)$$

$\mathcal{D}$  is the set of laws on paths, which coincide with the  $N$  temporal marginals at their respective times.  $\mathcal{A}$  is the set of laws given by linear additive noise SDEs. To find the underlying linear additive noise SDE in the intersection  $\mathcal{A} \cap \mathcal{D}$ , our method alternates between information projections,  $\arg \min_{q \in \mathcal{D}} D_{KL}(q \parallel p)$  and moment projections,  $\arg \min_{p \in \mathcal{A}} D_{KL}(q \parallel p)$ . The information projection step corresponds to trajectory inference, whose goal is to find the law on paths  $q \in \mathcal{D}$ , which

best aligns with the reference measure  $p$ . The moment projection then corresponds to maximum likelihood parameter estimation, since it amounts to determining the law on paths  $p \in \mathcal{A}$  over linear additive noise SDEs, which best aligns with the law of the estimated trajectories  $q$ . Indeed, in the infinite-data limit, MLE is equivalent to minimizing relative entropy, i.e. KL divergence (Akaike, 1998; White, 1982). At the population level, an iteration entails the updates:

$$q^{(k)} = \arg \min_{q \in \mathcal{D}} D_{KL}(q \| p_{A^{(k-1)}, H^{(k-1)}}) \quad (18)$$

$$A^{(k)} = \arg \min_{A \in \mathbb{R}^{d \times d}} D_{KL}(q^{(k)} \| p_{A, H^{(k-1)}}) \quad (19)$$

$$H^{(k)} = \arg \min_{H \in S_{\geq 0}^d} D_{KL}(q^{(k)} \| p_{A^{(k)}, H}). \quad (20)$$

At iteration  $k$ , we start by using the SDE parameters estimated from the previous iteration to define a reference SDE  $p_{A^{(k-1)}, H^{(k-1)}} \in \mathcal{A}$ . Using this reference SDE and the set of observed temporal marginals, we perform trajectory inference (18), to estimate the path distribution  $q^{(k)} \in \mathcal{D}$  that minimizes relative entropy to the reference SDE, while satisfying the marginal constraints (16) (see the middle plot of Figure 3). We then perform a two-step maximum likelihood estimation, in order to estimate the drift and diffusion from the estimated trajectories. This in turn updates the reference SDE  $p_{A^{(k)}, H^{(k)}} \in \mathcal{A}$  for the next iteration. To perform APPEX on a general additive noise SDE (2), the spaces  $\mathcal{A}$  and the drift maximum likelihood parameter estimation step (19) would be modified accordingly. We show in Corollary 22 of the appendix that there is a closed form diffusion MLE for general additive noise SDEs, once the drift has been estimated.

Previous works implement similar iterative schemes (Zhang, 2024; Shen et al., 2024b; Vargas et al., 2021), which alternate between trajectory inference and MLE parameter estimation. In contrast to our method, each of these works assumes that the diffusion of the process is known, and hence invariant across iterations. One reason for this assumption is to ensure finite KL divergence between the estimated trajectories and estimated SDEs for all iterations (Vargas et al., 2021). Given continuously observed marginals of a  $d$ -dimensional process, the KL divergence between two laws on paths  $q, p$  is taken over the path space  $\Omega = C([0, T], \mathbb{R}^d)$ , such that

$$D_{KL}(q \| p) = \int_{\Omega} \log \left( \frac{dq}{dp}(\omega) \right) dq(\omega).$$

Thus,  $D_{KL}(q \| p)$  will only be finite between two laws on paths if we can define the Radon-Nikodym derivative  $\frac{dq}{dp}$  over path space  $\Omega$ . By Girsanov's theorem, this is only ensured when both processes share the same diffusion (Shen et al., 2024b; Vargas et al., 2021). However, if we only consider measurements from a finite number of observed marginals, the KL divergence of the discretized processes  $q^N, p^N$  over the path space projected on the  $N$  measurement times,  $\Sigma_{\mathcal{D}} = C(\{t_i\}_{i=0}^{N-1}, \mathbb{R}^d)$ , can be decomposed as follows, see Benamou et al. (2019):

$$D_{KL}(q^N \| p^N) = \sum_{i=0}^{N-2} D_{KL}(q_{i,i+1} \| p_{i,i+1}) - \sum_{i=1}^{N-2} D_{KL}(q_i \| p_i), \quad (21)$$

where  $p_{i,i+1}, q_{i,i+1}$  are the joint probability measures of  $q, p$ , restricted to times  $t_i$  and  $t_{i+1}$ , and similarly  $q_i, p_i$  are the marginals of  $q, p$  at time  $t_i$ . We note that  $D_{KL}(q_i \| p_i) \leq D_{KL}(q_{i,i+1} \| p_{i,i+1})$  holds by the data-processing inequality. Hence,  $D_{KL}(q^N \| p^N)$  will be finite as long as  $D_{KL}(q_{i,i+1} \| p_{i,i+1}) = \int_{\mathbb{R}^d \times \mathbb{R}^d} \log \left( \frac{dq_{i,i+1}}{dp_{i,i+1}}(x) \right) q_{i,i+1}(x) dx < \infty$  for each  $i = 0, \dots, N-1$ . In particular, if  $p$  and  $q$  are the laws of two different drift-diffusion SDEs with distinct non-degenerate diffusions, then the KL divergence  $D_{KL}(q^N \| p^N)$  over the discretized path space  $\Sigma_{\mathcal{D}}$  will be finite. Since we consider a setting with a finite number of temporal marginal observations in this work, we may consider laws on

paths discretized over these observations. This allows us to both consider diffusions which are not known in advance, and to improve our diffusion estimates with respect to KL divergence after each iteration.

#### 4.1 Trajectory inference via anisotropic entropy-regularized optimal transport

To begin each iteration of APPEX, we infer trajectories given the set of temporal marginals  $\{p_i\}_{i=0}^{N-1}$  and a reference SDE  $p_{A^{(k-1), H^{k-1}}} \in \mathcal{A}$ , by solving an associated Schrödinger Bridge problem. Under certain conditions, the SB problem (5) can be solved using the variational entropic optimal transport (EOT) formulation

$$\pi^* = \arg \min_{\pi \in \Pi(\mu, \nu)} \int c(x, y) d\pi(x, y) + \epsilon^2 D_{KL}(\pi \| \mu \otimes \nu). \quad (22)$$

Intuitively,  $\pi^*$  transports the probability measure  $\mu$  to  $\nu$  while minimizing a total cost, based on the function  $c(x, y)$  and the entropic regularization  $\epsilon^2 > 0$ . Objectives (5) and (22) are equivalent (Peyré et al., 2019; Zhang, 2024), under the reference measure  $d\mathcal{K}(x, y) = K(x, y)d\mu(x)d\nu(y)$  with density  $K(x, y) \propto e^{\frac{c(x, y)}{\epsilon^2}}$ . The convention in the literature is to set  $c(x, y) = \frac{\|y - x\|^2}{2}$ , to define an isotropic Gaussian law  $\mathcal{K}$  (Janati et al., 2020; Lavenant et al., 2021; Chizat et al., 2022; Zhang, 2024). The EOT problem (22) can then be solved via Sinkhorn's algorithm.

However, the standard EOT problem (22) only considers a scalar regularization parameter  $\epsilon^2$ , which means that it can only directly model reference SDEs with isotropic diffusion (see Remark 21 in the appendix). To generalize trajectory inference for SDEs with anisotropic diffusion, we formalize “anisotropic entropy-regularized optimal transport” (AEOT), by considering transition kernels  $K$  with custom mean and covariance, e.g. parameterizing  $K$  with  $A$  and  $H = GG^\top$  rather than the scalar  $\epsilon^2 > 0$ . Indeed, we can consider more general Gaussian transition kernels,  $K_\theta(x, y) = \exp\left(\frac{(y - \mu(x, \theta))^\top \Sigma(\theta)^{-1} (y - \mu(x, \theta))}{2}\right)$ , in order to model a transition  $y|x \sim \mathcal{N}(\mu(x, \theta), \Sigma(\theta))$ , whose covariance  $\Sigma(\theta)$  is possibly anisotropic. Under this formulation, the cost is given by the inner product  $c_\theta(x, y) = \frac{(y - \mu(x, \theta))^\top \Sigma(\theta)^{-1} (y - \mu(x, \theta))}{2}$ . Trajectory inference would amount to solving the AEOT problem:

$$\pi^* = \arg \min_{\pi \in \Pi(\mu, \nu)} \int \frac{(y - \mu(x, \theta))^\top \Sigma(\theta)^{-1} (y - \mu(x, \theta))}{2} d\pi(x, y) + D_{KL}(\pi \| \mu \otimes \nu), \quad (23)$$

where the entropic regularization is captured in the matrix  $\Sigma(\theta)$  and function  $\mu(x, \theta)$ . The AEOT problem over a pair of marginals (23) can be solved via Sinkhorn's algorithm with inputs  $\mu, \nu, K_\theta$ . Proposition 20 in the Appendix then shows that the solution to the multi-marginal trajectory inference step (18) is the joint distribution given by the Markov concatenation of couplings (see Definition 19 in the Appendix)

$$\pi^* = \pi_{0,1} \circ \dots \circ \pi_{N-2, N-1},$$

where  $\pi_{i,i+1}$  is the AEOT solution (23) with marginals  $\mu = p_i, \nu = p_{i+1}$  and a transition kernel determined by the reference SDE.

**Remark 6 (Application to empirical marginals)** *Proposition 20 is formalized for exact temporal marginals  $p_i$ . However, in practice, we observe empirical measures  $\hat{p}_i$ , which converge in distribution to  $p_i$ , in the limit of infinite data. It is for these empirical measures  $\hat{p}_i$  which we actually compute the estimated couplings  $\hat{\pi}_{i,i+1}$  in practice. This corresponds to numerically estimating the AEOT solution*

$$\hat{\pi}_{i,i+1} = \arg \min_{\pi \in \Pi(\hat{p}_i, \hat{p}_{i+1})} \int \frac{(y - \mu(x, \theta))^\top \Sigma(\theta)^{-1} (y - \mu(x, \theta))}{2} d\pi(x, y) + D_{KL}(\pi \| \hat{p}_i \otimes \hat{p}_{i+1}). \quad (24)$$

By the main theorem in Ghosal et al. (2022), it holds that  $\hat{\pi}_{i,i+1}$  converges in distribution almost surely to the minimizer of (23) with  $\mu = p_i$  and  $\nu = p_{i+1}$  as the number of samples goes to infinity for each time  $i$  and  $i+1$ . Combining this with the previous proposition, we see that estimating (24) for each pair of times  $i$  and  $i+1$  is asymptotically equivalent to the KL minimization step in (18).

We also note that (24) is practically solved using Sinkhorn's algorithm with empirical marginals  $\hat{p}_i, \hat{p}_{i+1}$  and the discretized transition kernel  $K_\theta$  of the reference SDE. For example, if we have  $M$  samples per empirical marginal, then  $\hat{p}_i \sim \text{Unif}(x_{t_i}^{(j)} : j = 1, \dots, M)$  and  $\hat{p}_{i+1} \sim \text{Unif}(x_{t_{i+1}}^{(j)} : j = 1, \dots, M)$  would both be discrete uniform distributions over their samples, and  $K_\theta \in \mathbb{R}^{M \times M}$  would be a square matrix, such that entry  $K_{\theta,j,k}$  is obtained by applying the given transition kernel on the data points  $x_{t_i}^{(j)}$  and  $x_{t_{i+1}}^{(k)}$ .

## 4.2 Parameter estimation via MLE

To optimize objectives (19) and (20) for each iteration of APPEX, we require maximum likelihood estimators for the SDE parameters, given multiple observed trajectories from  $[0, T]$ . In the context of iteration  $k$  of APPEX, these are the trajectories sampled from the law on paths  $q^{(k)}$  obtained from the trajectory inference step. We derive closed-form maximum likelihood estimators for the linear additive noise SDE from Equation 3, given multiple trajectories in Proposition 7. Closed form drift MLE solutions are generally unavailable for additive noise SDEs, however we derive a closed form diffusion estimate (which depends on the drift) for general additive noise SDEs in Corollary 22 of the appendix.

**Proposition 7 (MLE estimators for drift and diffusion of SDE (3) from multiple trajectories)**

Given  $M$  trajectories over  $N$  equally spaced times:  $\{X_{i\Delta t}^{(j)} : i \in 0, \dots, N-1, j \in 0, \dots, M-1\}$  sampled from the linear additive noise SDE (3), the maximum likelihood solution for linear drift is approximated by

$$\hat{A} = \frac{1}{\Delta t} \left( \sum_{i=0}^{N-2} \sum_{j=0}^{M-1} (\Delta X_i^{(j)}) X_i^{(j)\top} \right) \left( \sum_{i=0}^{N-2} \sum_{j=0}^{M-1} X_i^{(j)} X_i^{(j)\top} \right)^{-1} \quad (25)$$

$$\xrightarrow{M \rightarrow \infty} \frac{1}{\Delta t} \left( \sum_{i=0}^{N-2} \mathbb{E}_{p_{i,i+1}}[(\Delta X_i) X_i^\top] \right) \left( \sum_{i=0}^{N-1} \mathbb{E}_{p_i}[X_i X_i^\top] \right)^{-1}, \quad (26)$$

where  $p_{i,i+1}$  is the joint measure over  $X_{t_i}$  and  $X_{t_{i+1}}$ . Similarly, the maximum likelihood solution for diffusion is approximated by

$$\hat{H} = \frac{1}{MT} \sum_{i=0}^{N-2} \sum_{j=0}^{M-1} (\Delta X_i^{(j)} - A X_i^{(j)} \Delta t) (\Delta X_i^{(j)} - A X_i^{(j)} \Delta t)^\top \quad (27)$$

$$\xrightarrow{M \rightarrow \infty} \frac{1}{T} \sum_{i=0}^{N-2} \mathbb{E}_{p_{i,i+1}}[(\Delta X_i - A X_i \Delta t) (\Delta X_i - A X_i \Delta t)^\top] \quad (28)$$

**Proof** See Section E of the Appendix. We note that estimators  $\hat{A}$  and  $\hat{H}$  were derived using the discretized transition kernel,  $X_{i+1}|X_i \sim \mathcal{N}(X_i + A X_i \Delta t, H \Delta t)$ . We derive the maximum likelihood estimators with the exact transition kernel  $X_{i+1}|X_i \sim \mathcal{N}(e^{A\Delta t} X_i, H \Delta t)$  in the one dimensional case in Section E.  $\blacksquare$

We note that the MLE drift estimator for  $A$  does not depend on the diffusion  $H$ , but the MLE estimator for  $H$  depends on  $A$ . We therefore estimate drift first in each iteration of APPEX.

### 4.3 The APPEX algorithm

We summarize APPEX's implementation in Algorithm 1. In each iteration, trajectory inference (18) is performed by solving the AEOT problem (23), and the drift and diffusion estimates are updated via MLE. By default, we use Sinkhorn's algorithm to solve AEOT and we use closed form MLE solutions when available.

---

**Algorithm 1** Parameter estimation for an additive noise SDE from temporal marginals with APPEX

---

```

1: Input: Observed marginals  $\hat{p}_i$ ,  $i = 0, \dots, N - 1$ , number of iterations  $K$ ,  $\Delta t$ 
2: Result: Estimated drift function  $\hat{b}$  and additive noise  $\hat{H}$ 
3: Initialize:  $\hat{b} \leftarrow 0$ ,  $H \leftarrow \sigma^2 I_d$ ,  $k \leftarrow 0$ 
4: while  $k < K$  do
5:   for  $i = 1, \dots, N$  do
6:      $\hat{\pi}_{i,i+1} \leftarrow$  Anisotropic-Entropy-Regularized-Optimal-Transport( $\hat{b}, \hat{H}, \hat{p}_{i-1}, \hat{p}_i, \Delta t$ )
7:   end for
8:   Sample-Trajectories  $\leftarrow \hat{\pi}_{N-1,N} \circ \dots \circ \hat{\pi}_{1,2}(p_0)$ 
9:    $\hat{b} \leftarrow$  MLEfit(Sample-Trajectories)
10:   $\hat{H} \leftarrow$  MLEfit(Sample-Trajectories,  $\hat{b}$ )
11:   $k \leftarrow k + 1$ 
12: end while
13:  $\mathcal{G} \leftarrow$  Estimate-Causal-Graph( $\hat{b}, \hat{H}, \epsilon$ )

```

---

**Remark 8 (Application to causal discovery)** As proven in Lemma 5 and visualized in Figure 1, the causal graph can be derived from the SDE parameters. For nonlinear drift  $b(X_t)$ , we include the edge  $i \rightarrow j$  if the  $j$ th component of the drift,  $b_j$ , is a function of  $X^{(i)}$ . For linear drift one may simply examine  $A_{j,i}$ . For multi-edges, one can check  $H_{i,j}$  to determine whether there is an unobserved confounder causing  $X^{(i)}$  and  $X^{(j)}$ . We therefore include a causal discovery step in line 13 of Algorithm 1. We acknowledge that many causal algorithms and independence tests are applicable, and leave the implementation as general as possible.

Because the trajectory inference and parameter estimation subprocedures are optimal with respect to minimizing KL divergence, we can show that APPEX's estimates reduce relative entropy to the true solution.

**Lemma 9** Suppose that  $A$  and  $H$  are the true drift and diffusion parameters of a linear additive noise SDE with temporal marginals  $p_0, \dots, p_{N-1}$ . Let  $q^{(k)} \in \mathcal{D}$  be the law of the estimated trajectories at iteration  $k$  of APPEX, and  $p_{A^k, H^k} \in \mathcal{A}$  be the law of the law of the estimated linear additive noise SDE, such that  $A^0 \in \mathbb{R}^{d \times d}$  and  $H^0 \in S_{\geq 0}^d$ . Then, the relative entropy between the estimated law of the trajectories and the law of the estimated linear additive noise SDE is decreasing with each iteration (Shen et al., 2024a):

$$D_{KL}(q^{(k+1)} \| p_{A^{k+1}, H^{k+1}}) \leq D_{KL}(q^{(k)} \| p_{A^k, H^k}) \quad \forall k \geq 0.$$

Furthermore, if  $p_0$  is not auto-rotationally invariant, then as the number of observed marginals  $N \rightarrow \infty$ , the relative entropy between the estimated law of the trajectories and the law of the estimated SDE is uniquely minimized by the underlying SDE  $p_{A, H}$ :

$$\inf_{q \in \mathcal{D}, p \in \mathcal{A}} D_{KL}(q \| p) = 0 \iff q = p = p_{A, H}$$

## Proof

Proposition 20 shows that  $q^{(k+1)} \in \mathcal{D}$  minimizes relative entropy to  $p_{A^k, H^k}$ . Similarly, any MLE solution  $p_{A^{(k+1)}, H^{(k+1)}}$  minimizes relative entropy to  $q^{(k+1)}$ . In particular, Proposition 7 approximates the MLE parameters  $A^{k+1} \in \mathbb{R}^{d \times d}$  and  $H^{(k+1)} \in S_{\geq 0}^d$ . By construction of the iterative scheme, we have that

$$D_{KL}(q^{(k+1)} \| p_{A^{(k+1)}, H^{(k+1)}}) \leq D_{KL}(q^{(k+1)} \| p_{A^{(k+1)}, H^{(k)}}) \leq D_{KL}(q^{((k+1))} \| p_{A^{(k)}, H^{(k)}}) \leq D_{KL}(q^{(k)} \| p_{A^{(k)}, H^{(k)}}),$$

which proves the first claim of the lemma. Then, by Theorem 3, if  $X_0$  is not auto-rotationally invariant, it follows that  $p_{A, H}$  is the law of the unique linear additive noise SDE, which obeys the marginal constraints  $p_0, \dots, p_{N-1}$  as  $N \rightarrow \infty$ . Equivalently, we have  $\mathcal{A} \cap \mathcal{D} = \{p_{A, H}\}$  and

$$\inf_{q \in \mathcal{D}, p \in \mathcal{A}} D_{KL}(q \| p) = 0 \iff q = p = p_{A, H},$$

■

Since  $D_{KL}(q^{(k)} \| p_{A^{(k)}, H^{(k)}})$  is non-increasing for successive iterations, this implies that the drift and diffusion estimates  $A^{(k)}, H^{(k)}$  progressively fit the data with each iteration. In this sense, our method approaches the true solution, which is unique, if the data is appropriately initialized and has sufficient observations.

## 5 Experiments

In a wide range of experiments on simulated data from linear additive noise SDEs, we find that APPEX accurately identifies the underlying SDE from its temporal marginals and that it outperforms the popular Waddington-OT method (Schiebinger et al., 2019). In Section 5.1, we assess the validity of Theorem 3 by showing that APPEX can learn the drift and diffusion parameters of classical non-identifiable SDEs, if  $X_0$  is not auto-rotationally invariant. We then demonstrate APPEX’s effectiveness on randomly generated higher-dimensional SDEs in Section 5.2. Finally, in Section 5.3, we show that APPEX can use its parameter estimates to recover the underlying causal graph, thus supporting Proposition 5. An empirical experiment for consistency is also provided in Appendix F, which shows that as the number of samples per time marginal increases, APPEX’s drift and diffusion estimates converge to the true parameters.

For each experiment, we simulate data for linear additive noise SDEs using Euler-Maruyama discretization with  $dt_{EM} = 0.01$ , such that we generate  $M = 500$  trajectories, each observed across 100 time steps. Each  $d$ -dimensional trajectory is initialized with  $p_0 \sim \text{Unif}\{x_i\}_{i=1}^d$  where  $\{x_i\}_{i=1}^d$  are random linearly independent vectors with each entry having a magnitude uniformly sampled between 2 and 10. It follows from Proposition 14 and Theorem 3, that this initial distribution ensures that the drift and diffusion are theoretically identifiable. To model the “marginals-only” setting, we subsample at the rate  $dt = 0.05$  to produce  $N = 20$  marginals with  $M = 500$  observations per time.

To perform parameter estimation, we use 30 iterations of our APPEX algorithm, such that the first reference SDE is an isotropic Brownian motion  $dX_t = \sigma dW_t$ , even when the true process has anisotropic noise. To model the realistic setting where diffusion is not precisely known, we assume that the initial guess of the diffusion’s trace is within an order of magnitude of the ground truth trace  $\text{tr}(H)$ . Specifically, we initialize  $A^{(0)} = 0, H^{(0)} = \sigma^2 I_d$  s.t.  $\sigma^2 \sim \text{tr}(H)10^{\text{Unif}(-1,1)}$ . Because the first reference SDE is  $\sigma dW_t$ , we note that the first iteration of APPEX is equivalent to performing MLE on trajectories that were inferred using the Waddington-OT (WOT) method from Schiebinger et al. (2019), based on standard entropy regularized OT (22) with  $\epsilon^2 = \sigma^2 \Delta t$ . APPEX and WOT are distinguished by the fact that APPEX benefits from further iterations, and allows the reference SDE to have anisotropic diffusion and non-zero drift. For each iteration of APPEX,

we use Sinkhorn’s algorithm to solve the anisotropic entropy-regularized optimal transport problem for trajectory inference, and we use the closed form MLE solutions from Proposition 7. Due to time complexity and numerical stability, we use linearized discretizations for the Gaussian transition kernels (unless  $d = 1$ ).

### 5.1 Revisiting non-identifiable SDEs

We consider three non-identifiable pairs of SDEs from the literature (summarized in Appendix A), but revise  $X_0$  to be non-auto-rotationally invariant. By Theorem 3, parameter estimation is feasible under the revised initial distribution. 10 replicates of each experiment were performed, such that the replicates featured data from different valid  $p_0$  initializations and different initial diffusivities  $\sigma^2$ . We track the mean absolute error (MAE), plotted in Figure 4, between the true drift/diffusion parameters and their estimates.

The results are consistent with Theorem 3 and Lemma 9. In each example, APPEX is able to estimate the drift and diffusion by iteratively improving upon both estimates, as evidenced by decreasing MAEs as the number of iterations increases. In particular, we observe the worst performance from the first iteration, which is equivalent to performing parameter estimation following trajectory inference by WOT. The most difficult SDE to infer was  $dX_t = -10X_t dt + \sqrt{10d}W_t$ , due to the high noise scale. We also note that APPEX succeeded in estimating the degenerate diffusion from the SDEs in Example 3, despite the fact that degenerate diffusion can result in infinite KL divergence with respect to a misspecified reference SDE.

### 5.2 Higher dimensional randomly generated linear additive noise SDEs

We now consider parameter estimation on a broad range of higher dimensional random linear additive noise SDEs. For each dimension  $d = 3, \dots, 10$ , we generate 10 random SDEs. To create each drift matrix  $A$ , we randomly sample each of its  $d^2$  entries from  $\text{Unif}(-5, 5)$ , and verify that its principal eigenvalue is less than 1. This allows us to consider non-stationary processes, while obeying reasonable growth conditions. To create each diffusion  $G$ , we randomly initialize each of its  $d^2$  entries via  $\text{Unif}(-1, 1)$  and then set  $H = GG^\top$ . For numerical stability, we perform Sinkhorn on the logarithmic scale for this experiment. We evaluate each estimate’s performance using MAE and correlation with the true parameters, where correlation is computed by vectorizing the corresponding matrices.

Dimension	A Estimation		$GG^\top$ Estimation	
	WOT	APPEX	WOT	APPEX
3	$0.351 \pm 0.04$	<b><math>0.237 \pm 0.04</math></b>	$0.793 \pm 0.205$	<b><math>0.147 \pm 0.030</math></b>
4	$0.730 \pm 0.067$	<b><math>0.328 \pm 0.041</math></b>	$1.549 \pm 0.439$	<b><math>0.415 \pm 0.070</math></b>
5	$0.912 \pm 0.060$	<b><math>0.602 \pm 0.195</math></b>	$2.174 \pm 0.702$	<b><math>0.362 \pm 0.039</math></b>
6	$1.43 \pm 0.170$	<b><math>0.358 \pm 0.020</math></b>	$18.010 \pm 8.636$	<b><math>0.256 \pm 0.046</math></b>
7	$1.480 \pm 0.132$	<b><math>0.360 \pm 0.015</math></b>	$6.807 \pm 1.724$	<b><math>0.345 \pm 0.037</math></b>
8	$1.862 \pm 0.137$	<b><math>0.460 \pm 0.015</math></b>	$5.472 \pm 1.266$	<b><math>0.359 \pm 0.019</math></b>
9	$1.803 \pm 0.222$	<b><math>0.487 \pm 0.016</math></b>	$8.134 \pm 3.024$	<b><math>0.454 \pm 0.122</math></b>
10	$1.670 \pm 0.241$	<b><math>0.439 \pm 0.019</math></b>	$35.122 \pm 28.529$	<b><math>0.317 \pm 0.025</math></b>

Table 1: Mean absolute error (MAE) of estimated drift and diffusion for dimensions 3-10.

The results demonstrate that APPEX estimates both SDE parameter sets robustly across all settings. Importantly, APPEX can handle arbitrary additive noise structures  $H = GG^\top$ , as evidenced by the fact that its drift and diffusion estimates have low MAE and high correlation with respect to the true parameters. This is significant because previous literature has focused on the

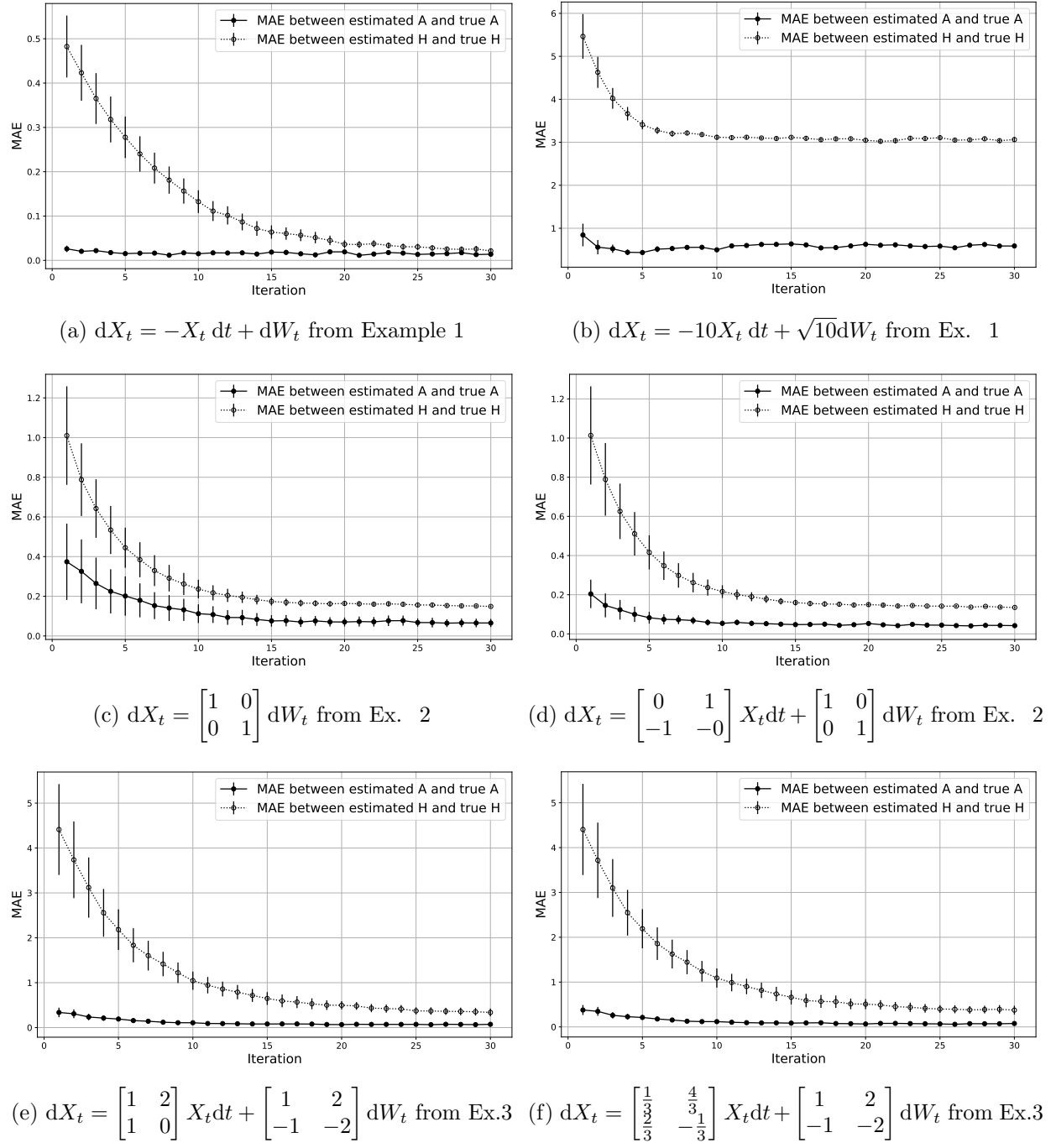


Figure 4: The mean absolute error for estimates of  $A$  and  $H$  using APPEX is shown per iteration for all three pairs of SDEs from Section A

setting of isotropic noise, but in practice, we expect correlated noise structures, as well as unequal noise along the main diagonal. In contrast, although WOT estimates the drift somewhat decently, it is unable to estimate the diffusion accurately, particularly in higher dimensions, since it is constrained to isotropic noise in its reference SDE. Figure 5 shows how APPEX is able to re-orient incorrect diffusion priors to closely match the true diffusion of the underlying SDE.

Dimension	A Estimation		$GG^\top$ Estimation	
	WOT	APPEX	WOT	APPEX
3	$0.996 \pm 0.001$	<b><math>0.998 \pm 0.001</math></b>	$0.837 \pm 0.048$	<b><math>0.985 \pm 0.005</math></b>
4	$0.943 \pm 0.015$	<b><math>0.987 \pm 0.005</math></b>	$0.729 \pm 0.039$	<b><math>0.865 \pm 0.031</math></b>
5	$0.921 \pm 0.016$	<b><math>0.952 \pm 0.030</math></b>	$0.728 \pm 0.040$	<b><math>0.909 \pm 0.018</math></b>
6	$0.794 \pm 0.040$	<b><math>0.986 \pm 0.001</math></b>	$0.530 \pm 0.056$	<b><math>0.961 \pm 0.007</math></b>
7	$0.792 \pm 0.029$	<b><math>0.988 \pm 0.001</math></b>	$0.595 \pm 0.037$	<b><math>0.946 \pm 0.012</math></b>
8	$0.699 \pm 0.035$	<b><math>0.981 \pm 0.002</math></b>	$0.611 \pm 0.042$	<b><math>0.949 \pm 0.006</math></b>
9	$0.740 \pm 0.033$	<b><math>0.978 \pm 0.002</math></b>	$0.615 \pm 0.025$	<b><math>0.919 \pm 0.033</math></b>
10	$0.760 \pm 0.049$	<b><math>0.983 \pm 0.001</math></b>	$0.641 \pm 0.041$	<b><math>0.960 \pm 0.006</math></b>

Table 2: Correlation between estimated and true drift and diffusion for dimensions 3-10.

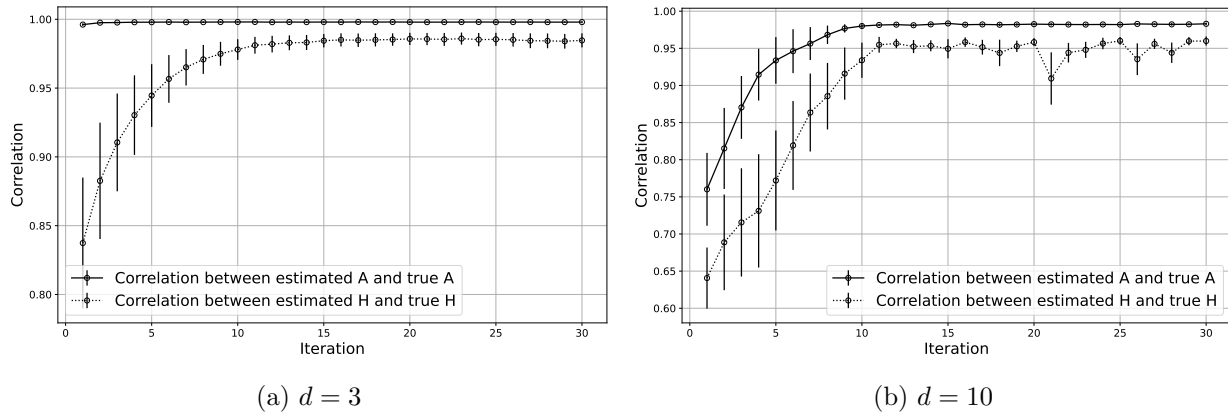


Figure 5: The correlation between the estimated and true SDE parameters is plotted per iteration across 10 random linear additive noise SDEs for dimensions 3 and 10

### 5.3 Causal discovery

We conclude with experiments that test our method's ability to recover the underlying causal graph. We first consider causal discovery from systems without latent confounders, and then consider causal discovery from systems with latent pairwise confounders through correlated diffusion.

In both settings, we generate random SDEs of dimension  $d = 3, 5, 10$  whose causal structure is determined by Erdős-Renyi graphs  $\mathcal{G}(d, p)$ , such that each of the  $d(d - 1)$  possible simple directed edges are included with probability  $p$ . As in Section 5.2, we ensure that the maximal eigenvalue of the randomly generated ground truth drift matrix is at most 1 to prevent unbounded growth. Proposition 5 states that simple directed edges  $e = i \rightarrow j \in E$  in the causal graph  $\mathcal{G} = ([d], E, \hat{E})$  are characterized by the condition  $A_{j,i} \neq 0$ . To simulate ground truth edges, we follow standard convention, by simulating edge weights  $A_{j,i}$  uniformly via  $\text{Unif}(-5, -0.5) \cup \text{Unif}(0.5, 5)$  (Runge, 2021; Reisach et al., 2021). We infer the presence of an edge  $i \rightarrow j$ , if in the estimated drift,  $\hat{A}_{j,i} > \epsilon$  (corresponding to a positive edge weight) or  $\hat{A}_{j,i} < -\epsilon$  (corresponding to a negative edge weight). We choose our threshold  $\epsilon = 0.5$  to match the minimal edge weight magnitude from our simulations. Inference of simple edges is then measured according to the structural Hamming distance between  $\mathcal{G}$  and the estimated graph  $\mathcal{G}_{est}$ , which considers the classification of positive directed edges, negative directed edges, and absent edges. The structural Hamming distance adds 1 for every misclassified simple edge:

$$d_{simple}(\mathcal{G}, \mathcal{G}) = \sum_{(i,j) \in [d] \times [d]} \mathbf{1} \left\{ \text{sgn}(A_{j,i}) \neq \text{sgn}(\hat{A}_{j,i}) \mathbf{1}_{|\hat{A}_{j,i}| > \epsilon} \right\}. \quad (29)$$

If the observed system does not have any latent confounders from correlated diffusion, we enforce this by setting the diffusion matrix  $G$  to be strictly diagonal. This ensures that the only edges in  $\mathcal{G}$  are simple edges from the drift. As in the experiments on random matrices, we set each of the  $d$  diagonal entries of  $G$  via  $\text{Unif}(-1, 1)$ . Conversely, when modeling pairwise latent confounders, we introduce correlated diffusion by selecting a random subset of columns in  $G$  to have precisely two nonzero entries. In particular, we initialize all entries along the diagonal of  $G$  to be 1, and for each of the selected columns, e.g. column  $i$ , we set one non-diagonal entry  $G_{i,j} = 1$ , to model the pairwise latent confounder  $U_{i,j}$ . All other entries are set to 0. The number of selected columns with pairwise latent confounders is sampled from  $\text{Unif}\{1, \dots, \lfloor 2d/3 \rfloor\}$ , e.g. we sample from  $\text{Unif}\{1, 2\}$  for  $d = 3$ ,  $\text{Unif}\{1, 2, 3\}$  for  $d = 5$ , and  $\text{Unif}\{1, \dots, 6\}$  for  $d = 10$ . Proposition 5 states that bidirected edges  $(i, j) \in \tilde{E}$  from pairwise latent confounders  $U_{i,j}$ , are characterized by the condition  $H_{i,j} = G_i \cdot G_j \neq 0$ . We infer the presence of  $U_{i,j}$ , if in the estimated diffusion,  $|\hat{H}_{i,j}| > \epsilon$ . We set  $\epsilon = 1$  to match the data construction  $(i, j) \in \tilde{E} \iff H_{i,j} = G_i \cdot G_j \geq 1$ . Inference of bidirected edges is measured according to the structural Hamming distance, which adds 1 for every misclassified bidirected edge:

$$d_{\text{latent}}(\mathcal{G}, \mathcal{G}_{\text{est}}) = \sum_{(i,j) \in [d] \times [d]: i \neq j} \mathbf{1} \left\{ (|H_{i,j}| > \epsilon \cap |\hat{H}_{i,j}| \leq \epsilon) \cup (|H_{i,j}| \leq \epsilon \cap |\hat{H}_{i,j}| > \epsilon) \right\}. \quad (30)$$

Table 3 reports the mean structural Hamming distances for simple edges from causal graphs estimated by WOT and APPEX, in the setting without latent confounders. APPEX outperforms WOT across all tested dimensions  $d \in \{3, 5, 10\}$  and edge probabilities  $p \in \{0.1, 0.25, 0.5\}$ , with the discrepancy becoming more pronounced as the causal structure grows in complexity at higher dimensions and edge densities. We observe that APPEX can consistently infer complex causal relationships, whereas WOT’s inference is often limited, due to mis-specified diffusion. For example, the first row in Figure 6 demonstrates that APPEX recovers the system’s negative feedback structure, while WOT introduces additional cycles in order to compensate for a poorly specified reference diffusion.

Table 4 reports the mean structural Hamming distances for simple and bidirected edges (from latent pairwise confounders) from causal graphs estimated by WOT and APPEX, in the setting with correlated diffusion. The probability  $p$  of connecting a simple directed edge  $i \rightarrow j$  was fixed at  $p = 0.25$ . As in the setting with uncorrelated diffusion, APPEX outperforms WOT in all evaluated settings, particularly for higher-dimensional systems.

Table 3: Average Structural Hamming Distance (lower is better) with varying dimensions and random edge probabilities  $p$ .

Dimension	$p = 0.1$		$p = 0.25$		$p = 0.5$	
	WOT	APPEX	WOT	APPEX	WOT	APPEX
3	$0.40 \pm 0.40$	<b><math>0.00 \pm 0.00</math></b>	$1.80 \pm 0.76$	<b><math>0.30 \pm 0.30</math></b>	$1.40 \pm 0.65$	<b><math>0.00 \pm 0.00</math></b>
5	$3.80 \pm 2.13$	<b><math>0.10 \pm 0.10</math></b>	$3.56 \pm 1.70$	<b><math>0.00 \pm 0.00</math></b>	$4.40 \pm 1.14$	<b><math>0.60 \pm 0.22</math></b>
10	$38.30 \pm 8.53$	<b><math>0.50 \pm 0.40</math></b>	$48.60 \pm 6.55$	<b><math>0.80 \pm 0.39</math></b>	$37.4 \pm 4.66$	<b><math>3.30 \pm 0.70</math></b>

## 6 Discussion

Many recent works have focused on inferring the drift or diffusion from an SDE’s temporal marginals, yet the problem of non-identifiability remained largely unaddressed (Weinreb et al., 2018; Lavenant et al., 2021; Chizat et al., 2022; Shen et al., 2024a; Zhang, 2024; Terpin et al., 2024; Brogat-Motte et al., 2024). To resolve this issue, we provide necessary and sufficient identifiability conditions for linear additive noise SDEs in Theorem 3. With this theorem, we prove that non-identifiability of the drift and diffusion arises precisely from the auto-rotational invariance of the initial distribution

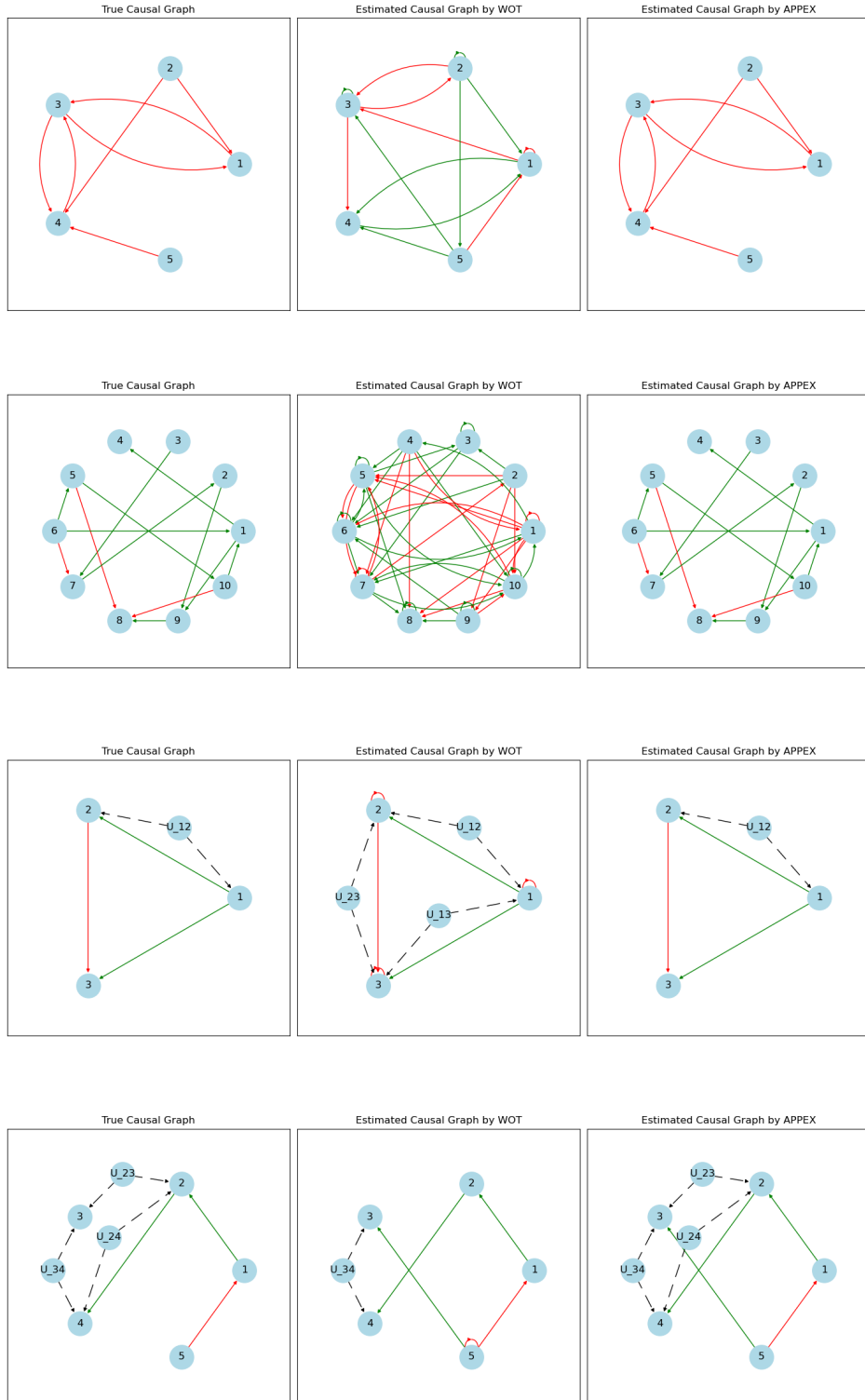


Figure 6: The true and estimated causal graphs by WOT and APPEX for four random SDEs of dimensions are illustrated. Red edges  $i \rightarrow j$  represent negative edge weights, such that  $X^{(i)}$  negatively regulates  $X^{(j)}$ . Green edges  $i \rightarrow j$  represent positive edge weights, such that  $X^{(i)}$  positively regulates  $X^{(j)}$ . Dashed edges represent the effect of a latent confounder  $U_{i,j}$  on observed variables  $i, j$  through correlated diffusion.

Table 4: Average Structural Hamming Distance for simple edges, and latent confounders (lower is better) with varying dimensions and random edge probability  $p = 0.25$ .

Dimension	Hamming distance for simple edges		Hamming distance for latent confounders	
	WOT	APPEX	WOT	APPEX
3	$1.20 \pm 0.51$	<b><math>0.7 \pm 0.40</math></b>	$1.00 \pm 0.30$	<b><math>0.00 \pm 0.00</math></b>
5	$4.80 \pm 1.47$	<b><math>1.60 \pm 0.87</math></b>	$3.50 \pm 0.64$	<b><math>0.10 \pm 0.10</math></b>
10	$38.00 \pm 6.30$	<b><math>3.00 \pm 0.77</math></b>	$23.80 \pm 3.86$	<b><math>2.90 \pm 1.39</math></b>

$X_0$ . We also show that the drift and diffusion parameters identify the underlying causal graph for general additive noise SDEs. This provides a theoretical foundation for learning the precise dynamics and causal structure of a linear additive noise process, solely from its temporal marginals, without relying on the usual prior knowledge assumptions and model restrictions.

To build on our theoretical contributions, we also introduce APPEX, a method that simultaneously learns drift and diffusion from temporal marginals. APPEX iterates towards the optimal parameter set by alternating between trajectory inference, via anisotropic entropy-regularized optimal transport, and MLE parameter estimation. Since each of these subprocedures are asymptotically optimal (Lemma 9), given a finite set of the process’ true marginals, APPEX improves its estimates with each iteration. When tested on hundreds of randomly generated linear additive noise SDEs between dimensions 3 to 10, APPEX is able to effectively recover the process’ drift, diffusion, and causal graph, while significantly outperforming Waddington-OT, which is one of the most popular inference methods in single-cell biology.

Our theoretical and algorithmic contributions offer a number of insights to advance statistical inference methods from temporal marginals. First, our framework removes common model restrictions to expand the set of dynamics that can be inferred from marginals. This includes negative feedback loops and repressilator dynamics, which both arise from rotational drift, and correlated noise, which arises from anisotropic diffusion. These features are common in real-world datasets, and are especially relevant for accurate trajectory and GRN inference from single-cell data (Weinreb et al., 2018; Santos et al., 2024). Second, we demonstrate that joint identification of the unique drift and diffusion parameters is theoretically and practically possible in the “marginals-only” setting. Previous and concurrent works either estimate only one parameter given the other (Weinreb et al., 2018; Lavenant et al., 2021; Chizat et al., 2022; Shen et al., 2024a; Zhang, 2024; Forrow, 2024) or estimate both without guaranteeing non-identifiability (Terpin et al., 2024; Brogat-Motte et al., 2024). We note that even if a user is only interested in one parameter, APPEX offers the ability to estimate it, regardless of how the other parameter is initialized. This is particularly significant given that a misspecified diffusion typically leads to a misidentified drift, and vice-versa. Third, we remark that the fundamental condition for identifiability is satisfied by a large class of distributions and should therefore be widely applicable. Indeed, the only pathological distributions are auto-rotationally invariant, which fall into three categories (see Figure 2): 1) satisfying invariance under a rotation after scaling and shearing, 2) having a mean-0 Gaussian cross-section, 3) having rank-degenerate support. One can therefore check the initial distribution, and perform an intervention if needed, to guarantee system identifiability from marginals generated by a linear additive noise SDE.

## 6.1 Limitations and future work

Although this paper presents several breakthroughs for the identification of SDEs from marginal snapshots, we acknowledge several limitations and opportunities for future work.

First, while Theorem 3 shows that identifiability is guaranteed when the initial distribution  $X_0$  is not auto-rotationally invariant, and that there exist non-identifiable SDEs if  $X_0$  is auto-rotationally

invariant, we note that this is distinct from the stronger claim that given a set of observed temporal marginals from an SDE, the true parameters are uniquely identifiable from the data if and only if  $X_0$  is auto-rotationally invariant. For example, if  $X_0$  is rotationally symmetric, e.g.  $N(0, I_d)$ , then it would be impossible to determine rotational drift. Similarly, if  $X_0$  is rank-degenerate, then it would be impossible to distinguish between drifts that each contain  $X_0$  in its nullspace. However, if the underlying SDE has rotational drift, and  $X_0$  is degenerate, then the ensuing marginals likely identify the SDE parameters. Similarly, a full rank rotationally symmetric  $X_0$  may identify the underlying SDE from the rank degeneracy counterexample. Importantly, the true SDE is generally unknown, so it is difficult to assess whether identifiability holds despite  $X_0$  being auto-rotationally invariant. For this reason, the strong guarantee of identifiability under non-auto-rotationally invariant  $X_0$  is practical.

Second, our identifiability result is restricted to time homogeneous linear additive noise SDEs. Although this is a popular model for real-world processes, including for GRN inference (Rohbeck et al., 2024; Zhang, 2024), it would be beneficial to characterize identifiability conditions under more general models. We note that characterizing identifiability is particularly challenging for non-additive noise models, where the noise depends on the process  $X_t$ , since the same marginal observations can be explained by a nonlinear additive noise SDE and a linear multiplicative noise SDE (Coomer et al., 2022). For this reason, it may be easier to consider identifiability for parameteric families of nonlinear drift under the additive noise model. We note that we have already proven results about causal discovery for additive noise SDEs in Section 3.2 and that APPEX is also formulated for general additive noise SDEs. Although the MLE for nonlinear drift may not have a closed form solution, optimizers like BFGS (Lavenant et al., 2021; Chizat et al., 2022; Wang et al., 2024) and neural networks (Shen et al., 2024a) have been successfully used for SDE parameter estimation on real and synthetic data.

Third, our theory considers the infinite data setting, given the process' true marginals  $\{p_i\}_{i=0}^{N-1}$ , and we have not studied asymptotic convergence rates. In particular, our identifiability result was established given continuously observed marginals, which corresponds to obtaining infinite samples from infinite marginals. Similarly, the theory surrounding the optimality of APPEX assumes that we have infinite samples from a finite set of marginals. We leave the asymptotic analysis of APPEX for future work. Directions for future work include the sample complexity of entropic optimal transport for trajectory inference, which requires asymptotically more samples per marginal as we decrease the entropic regularization (decreasing time granularity in the SDE setting) (Genevay et al., 2019)[Thm. 3], and the fact that the MLE of the AR(1) process from multiple trajectories is slightly biased (Ledolter, 2009). We note that APPEX could be combined with previous methods that relax the marginal constraints (see Lavenant et al. (2021)). This could improve estimates in low data settings, particularly in the biological setting where taking measurements destroys samples.

Fourth, even in the asymptotic setting, the nonconvex nature of APPEX's alternating projection optimization problem makes the prospect of proving convergence difficult. Although our experiments indicate that APPEX's estimates approach the true solution, regardless of the initial guesses for the drift  $A$  and observational diffusion  $H$ , we have not yet proved convergence due to the non-convexity of the optimization space. A formal proof of convergence and consistency would further strengthen APPEX's theoretical foundation.

Finally, we note that the trajectory inference step of APPEX, which we solve using Sinkhorn's algorithm, is computationally intensive. When solving the standard EOT problem (22), the asymptotic computation of each iteration of Sinkhorn's algorithm is  $O(\frac{N^2}{\epsilon^3})$ , where  $N$  is the number of samples, and  $\epsilon$  is the scalar entropy regularization (Altschuler et al., 2017). The number of iterations required is further related to the average error, which decays like  $O(\frac{1}{\sqrt{N\epsilon^d}})$  (Genevay et al., 2019). Similar asymptotics hold for the AEOT problem (23). We note that accurate trajectory inference relies on a large number of samples ( $N$ ), a small entropic regularization  $\epsilon^2 \sim \delta t$ , and potentially high-dimensional data. Our method is therefore impractical on very large datasets, which

are prevalent in biological applications. It would therefore be advantageous to solve the associated Schrodinger bridge problem using more efficient methods. We note that recent work makes use of closed form solutions to the SB problem when  $X_0$  is a degenerate Dirac distribution, to increase computational efficiency (Huang, 2024). We also note that the SB problem can be expressed via forwards and backwards drifts (Vargas et al., 2021), and can therefore be solved via generative diffusion models (De Bortoli et al., 2021; Shi et al., 2024). Thus, when a closed form solution is not known, generative diffusion models may be more efficient solvers for the trajectory inference problem. Concurrent work estimates drift and diffusion using other methods, including JKO energy minimization (Terpin et al., 2024) and reproducing Hilbert kernel spaces to minimize distance to the Fokker-Planck solution (Brogat-Motte et al., 2024). We have not yet compared the accuracy and computational efficiency of these methods against APPEX, and a systematic comparative analysis would be an interesting direction for future research.

## Code Availability

The Python code for reproducing the experimental results and figures is available at <https://github.com/guanton/APPEX>. Analogous code in R is available at <https://github.com/HydroML/X0isAllYouNeed>.

## Acknowledgments and Disclosure of Funding

The authors would like to thank United Therapeutics for supporting this research. GS and AW also acknowledge the support of the Burroughs Wellcome Fund.

## Appendix A. Non-identifiable linear additive noise SDEs

We summarize three classical examples of non-identifiability from the literature (Lavenant et al., 2021; Shen et al., 2024b; Wang et al., 2024; Hashimoto et al., 2016; Weinreb et al., 2018). In all examples, the processes  $X_t$  and  $Y_t$  share the same time marginals.

### Example 1 (Starting at stationary distribution (Lavenant et al., 2021; Shen et al., 2024b))

*This example is motivated by the fact that multiple SDEs share the same stationary distribution. Hence, if  $p_0$  is initialized at the stationary distribution, then these SDEs will be non-identifiable from their marginals. We provide a simple example.*

$$dX_t = -X_t dt + dW_t, \quad X_0 \sim \mathcal{N}(0, \frac{1}{2}) \quad (31)$$

$$dY_t = -10Y_t dt + \sqrt{10}dW_t, \quad Y_0 \sim \mathcal{N}(0, \frac{1}{2}) \quad (32)$$

Here, both SDEs have the same stationary distribution  $\mathcal{N}(0, \frac{1}{2})$  despite having significantly different individual trajectories. Indeed, the stationary distribution of a 1-dimensional 0-mean Ornstein-Uhlenbeck (OU) process with drift  $-\lambda X_t$  and diffusion  $\sigma$  is  $\mathcal{N}(0, \frac{\sigma^2}{2\lambda})$ , which depends only on the drift:diffusivity ratio  $\lambda/\sigma^2$  (Lavenant et al., 2021). For multivariate OU processes with drift  $A$  and observational diffusion  $H$ , the stationary distribution  $\mathcal{N}(0, \Sigma)$  depends only on the relationship  $\Sigma A + A\Sigma = -H$  (Mandt et al., 2016). Intuitively, the set of OU processes, which share the same stationary distribution  $\mathcal{N}(0, \Sigma)$  are equivalent up to rescaling time. We note that this example also generalizes easily to the case where one component of  $X_0$  is mean-0 Gaussian, i.e.  $(PX_0)_1 \sim \mathcal{N}(0, \sigma^2)$ .

### Example 2 (Rotation around process mean (Shen et al., 2024b; Hashimoto et al., 2016))

*In this example, the first SDE governing  $X_t$  is 2-dimensional Brownian motion and the second SDE governing  $Y_t$  adds a divergence-free rotational vector field  $(x, y) \rightarrow (y, -x)$  about  $(0, 0)$ , which is undetectable if the initial distribution  $p_0$  is rotationally invariant.*

$$dX_t = dW_t, \quad X_0 \sim \mathcal{N}(0, Id) \quad (33)$$

$$dY_t = \begin{bmatrix} 0 & 1 \\ -1 & 0 \end{bmatrix} Y_t dt + dW_t, \quad Y_0 \sim \mathcal{N}(0, Id) \quad (34)$$

Hence, if  $p_0$  is an isotropic distribution with mean  $(0, 0)$ , then  $X_t$  and  $Y_t$  are non-identifiable from one another (Shen et al., 2024b). This can also be shown directly with the Fokker-Planck equation (4), since  $\nabla \cdot (Ax)p(x, t) = \nabla p(x, t) \cdot Ax + p(x, t)\nabla \cdot A(x) = \nabla p(x, t) \cdot Ax = 0$ , if  $p$  is parallel to the rotational vector field  $Ax = \begin{bmatrix} 0 & 1 \\ -1 & 0 \end{bmatrix} x$ .

**Example 3 (Degenerate rank (Wang et al., 2024))** *In this example motivated by Wang et al. (2024), trajectories (and therefore temporal marginals) of distinct SDEs are non-identifiable if the process is degenerate, limiting observations to a strict subspace of  $\mathbb{R}^d$ .*

$$dX_t = \begin{bmatrix} 1 & 2 \\ 1 & 0 \end{bmatrix} X_t dt + \begin{bmatrix} 1 & 2 \\ -1 & -2 \end{bmatrix} dW_t, \quad X_0 = \begin{bmatrix} 1 \\ -1 \end{bmatrix} \quad (35)$$

$$dY_t = \begin{bmatrix} 1/3 & 4/3 \\ 2/3 & -1/3 \end{bmatrix} Y_t dt + \begin{bmatrix} 1 & 2 \\ -1 & -2 \end{bmatrix} dW_t, \quad Y_0 = \begin{bmatrix} 1 \\ -1 \end{bmatrix} \quad (36)$$

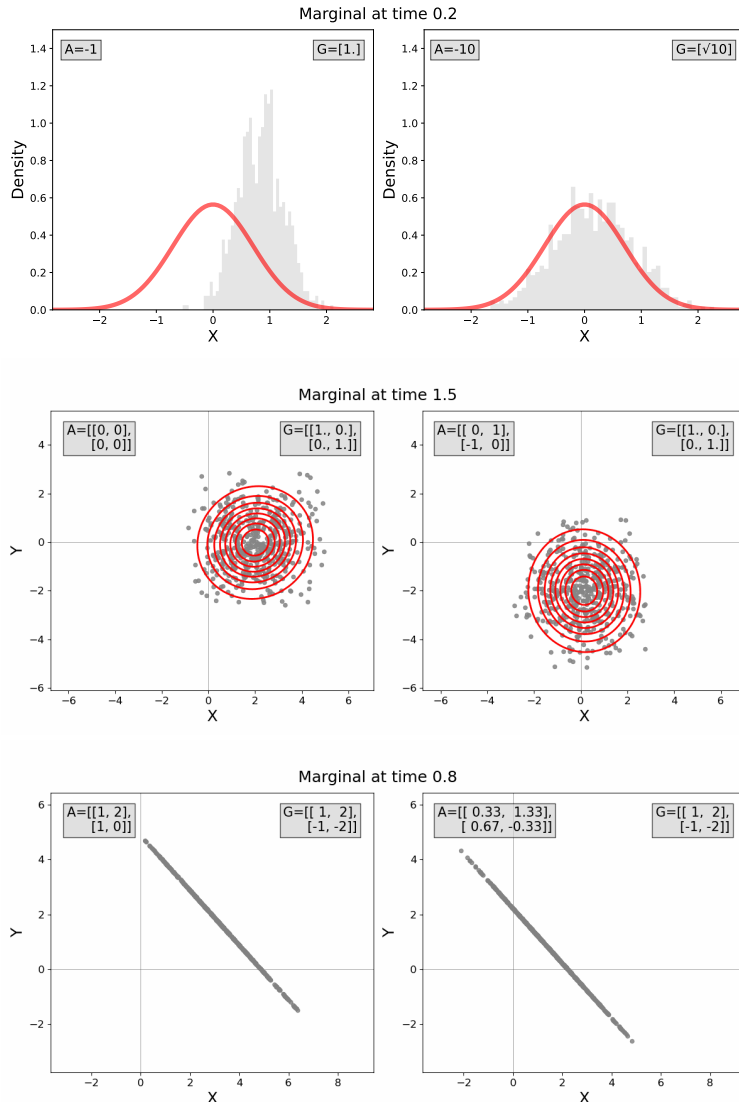
The drift matrices  $\begin{bmatrix} 1 & 2 \\ 1 & 0 \end{bmatrix}, \begin{bmatrix} 1/3 & 4/3 \\ 2/3 & -1/3 \end{bmatrix}$  each have eigenvector  $X_0 = \begin{bmatrix} 1 \\ -1 \end{bmatrix}$  with eigenvalue  $-1$ .

Moreover, the diffusion is rank-degenerate with column space  $\text{span}(\begin{bmatrix} 1 \\ -1 \end{bmatrix})$ . Thus, both SDEs will

have identical behaviour along  $\text{span}(\begin{bmatrix} 1 \\ -1 \end{bmatrix})$  and are only differentiated by their behaviour elsewhere.

Given  $X_0 = \begin{bmatrix} 1 \\ -1 \end{bmatrix}$ , the processes will stay within  $\text{span}(\begin{bmatrix} 1 \\ -1 \end{bmatrix})$  and are non-identifiable from one another. We note that this non-identifiability holds even when we observe trajectories (Wang et al., 2024), whereas the first two examples are identifiable from trajectories but not identifiable from marginals.

Theorem 3 proves that identifiability in the “marginals-only” setting is guaranteed for linear additive noise SDEs if  $X_0$  is not auto-rotationally invariant. Figure 7 demonstrates how non-auto-rotationally invariant initial distributions  $X_0$  resolves these classical non-identifiable examples from the literature.



(a) This corresponds to Example 1 with  $X_0 \sim \delta_1$ . The SDE with drift  $A = H = 10$  (right) has converged to the stationary distribution (red) at time  $t = 0.2$ , while the SDE with  $A = H = 1$  (left) has not yet sufficiently drifted or diffused.

(b) This corresponds to Example 2, with  $X_0 \sim \text{Unif}\{(2, 0), (2, 0.1)\}$ . The first SDE is irrotational and maintains mean  $(2, 0.05)$ . The second SDE (right) rotates about the origin. At time  $t = 1.5$ , the mean has shifted to approximately  $(0, -2)$ .

(c) This corresponds to Example 3, with  $X_0 \sim \text{Unif}\{(1, 0)^\top, (0, 1)^\top\}$ . The first SDE (left) has eigenvalue 2 for  $(2, 1)$ , while the second (right) has eigenvalue 1, leading to more extreme intercepts in the left plot at  $t = 0.8$ .

Figure 7: Marginals are plotted at various times for the SDE pairs from Section 3 of the Appendix, following various non-auto-rotationally invariant initial distributions.

### A.1 Properties of the Linear Additive Noise SDE

Let  $X_t$  evolve according to a linear additive noise SDE (3). Then its solution can be obtained using the integrating factor  $e^{-At}$  (Särkkä and Solin, 2019)[Sec 4.3] and is given by

$$X_t = e^{At} X_0 + \int_0^t e^{A(t-s)} G dW_s \quad (37)$$

By the independent increments of  $W_t$ , we may interpret  $X_t$  as being composed of two independent r.v.'s. The first is a time-dependent function of its initial distribution,  $e^{At} X_0$ , and the second is a mean-0 Gaussian  $\mathcal{N}(0, \Sigma_t)$  with time-dependent variance  $\Sigma_t = \int_0^t e^{A(t-s)} H e^{A^\top(t-s)} ds$ . It follows that the exact transition kernel of a linear additive noise SDE satisfies  $X_{t+\Delta t} | X_t \sim \mathcal{N}(\mu_t, \Sigma_t)$ , where  $\mu_t = e^{A\Delta t} X_t$  (Zhang, 2024). The linearized transition kernel is given by  $\mathcal{N}(X_t + A X_t \Delta t, H \Delta t)$ .

### A.2 Weak formulation of the Fokker-Planck equation

We may define the linear operator  $\mathcal{L}$

$$(\mathcal{L}f)(x) = b(x) \cdot f(x) + \frac{1}{2} \nabla \cdot (H \nabla f(x)),$$

$\mathcal{L}$  is the generator of the additive noise SDE (2) (Holmes-Cerfon, 2015). Its adjoint operator is given by

$$(\mathcal{L}^* g)(x) = -\nabla \cdot (b(x, t) g(x)) + \nabla \cdot (H \nabla g(x)).$$

and satisfies

$$\int_{\mathbb{R}^d} \mathcal{L}f(x)g(x) dx = \langle \mathcal{L}f, g \rangle = \langle f, \mathcal{L}^* g \rangle = \int_{\mathbb{R}^d} f(x) \mathcal{L}^* g(x) dx,$$

for all smooth and compactly supported test functions  $f, g \in C_c^\infty(\mathbb{R}^d)$ .

Then, the Fokker-Planck equation can be formulated in the weak sense as follows. For each  $t \geq 0$  let  $p_t$  be a probability measure on  $\mathbb{R}^d$  and assume that  $t \mapsto p_t$  is narrowly continuous. Then we say  $p_t$  solves the Fokker-Planck equation in the weak sense provided that

$$\frac{d}{dt} \int \varphi(x) dp_t(x) = \int \mathcal{L}\varphi(x) dp_t(x) \quad \forall \varphi \in C_c^2(\mathbb{R}^d). \quad (38)$$

This weak formulation accommodates the case where  $b$  is not differentiable and  $p_t$  is not necessarily absolutely continuous with respect to the Lebesgue measure. For  $p_t$  with sufficiently regular Lebesgue density  $p(x, t)$  this weak solution concept is equivalent to the classical sense of the Fokker-Planck equation, i.e.

$$\partial_t p(x, t) = \mathcal{L}^* p(x, t).$$

For the measure-theoretic weak formulation of the Fokker-Planck equation, we quote the following existence and uniqueness results from Stroock (2008). Under our standing assumptions on the drift and diffusion coefficients (namely: the drift is linear, and the diffusion is constant but possibly degenerate), by Theorem 1.1.9 in Stroock (2008), weak solutions to the Fokker-Planck equation exist whenever the initial condition  $\rho_0$  has finite second moments; and moreover, by Theorem 2.2.9 in Stroock (2008), the solution is unique provided that all moments of  $\rho_0$  are finite.

### A.3 Properties of auto-rotationally invariant r.v.s

**Lemma 10** *Let  $\Sigma \succ 0$  and  $A \in \mathbb{R}^{d \times d}$  be such that*

$$A\Sigma + \Sigma A^\top = 0.$$

*Then,  $B = \Sigma^{1/2} A \Sigma^{-1/2}$  is skew-symmetric, and for all  $t \in \mathbb{R}$ ,*

$$e^{At} = \Sigma^{-1/2} e^{Bt} \Sigma^{1/2}.$$

*In other words, the  $\Sigma$ -generalized rotation  $e^{At}$  produces a classical rotation  $e^{Bt}$  after the change of variables  $y = \Sigma^{1/2}x$ , which can be interpreted as a shearing and scaling transformation of  $\mathbb{R}^d$ .*

**Proof** Since  $\Sigma \succ 0$ , the unique symmetric positive definite square root  $\Sigma^{1/2}$  exists and is invertible. Define

$$B = \Sigma^{-1/2} A \Sigma^{1/2}, \quad B^\top = \Sigma^{1/2} A^\top \Sigma^{-1/2}.$$

Then, since  $A\Sigma + \Sigma A^\top = 0$ , we can multiply on the left by  $\Sigma^{-1/2}$  and on the right by  $\Sigma^{-1/2}$  to yield

$$0 = \Sigma^{-1/2} A \Sigma^{1/2} + \Sigma^{1/2} A^\top \Sigma^{-1/2} = B + B^\top,$$

which proves that  $B$  is skew-symmetric, and therefore  $e^{Bt}$  defines a classical rotation in  $\mathbb{R}^d$ , such that

$$e^{Bt} = e^{\Sigma^{-1/2} A \Sigma^{1/2}} = \Sigma^{-1/2} e^{At} \Sigma^{1/2},$$

where the last equality can be seen by writing  $e^{Bt} = \sum_{n=0}^{\infty} t^n \frac{B^n}{n!}$  and noting that  $B^n = (\Sigma^{-1/2} A \Sigma^{1/2})^n = \Sigma^{-1/2} A^n \Sigma^{1/2}$ . Rearranging yields  $e^{At} = \Sigma^{-1/2} e^{Bt} \Sigma^{1/2}$  as desired.

To explicitly see that the change of variable  $y = \Sigma^{1/2}x$  amounts to a shearing and scaling, note that any positive definite matrix admits an  $LDL^\top$  factorization:

$$\Sigma = L D L^\top,$$

where  $L$  is unit lower-triangular (so its off-diagonal entries describe a shear transformation) and  $D$  is a diagonal matrix with positive entries (representing scaling along the coordinate axes). Thus, the transformation  $x \mapsto y = \Sigma^{1/2}x$  decomposes into a shear (via  $L$ ) and a scaling (via  $D^{1/2}$ ). ■

**Lemma 11** *Let  $X$  be a r.v. with covariance  $\Sigma$  and suppose that  $e^{At}X \sim X$  for all  $t \geq 0$ . Then,  $A\Sigma + \Sigma A^\top = 0$ . Moreover, we have the identity*

$$\int_0^t e^{A(t-s)} \Sigma e^{A^\top(t-s)} ds = t\Sigma. \quad (39)$$

**Proof** Let  $C(t) = \text{Cov}(e^{At}X)$ .  $e^{At}X \sim X$  implies that for all  $t \geq 0$ , the covariance  $C(t)$  stays constant, such that  $C(t) = \text{Cov}(X) = \Sigma$ . Directly computing  $C(t)$  and its derivative yields

$$\begin{aligned} C(t) &= e^{At} \Sigma e^{A^\top t} = \Sigma \\ C'(t) &= Ae^{At} \Sigma e^{A^\top t} + e^{At} \Sigma A^\top e^{A^\top t} = 0 \end{aligned}$$

and we plug in  $t = 0$  to get the first claim

$$C'(0) = A\Sigma + \Sigma A^\top = 0.$$

■

**Lemma 12** Let  $\text{Cov}(X) = \Sigma \succ 0$  and suppose that  $e^{At}X \sim X$  for some  $A \neq 0$ . Then  $X$  admits a density, and the level sets of its probability density function are  $\Sigma$ -rotationally invariant ellipsoids:

$$\text{Let } E_{\Sigma}^{(k)} = \{x \in \mathbb{R}^d : x^{\top} \Sigma^{-1} x = k\}, \text{ then } \forall x, y \in E_{\Sigma}^{(k)}, p(x) = p(y) \quad (40)$$

**Proof** Since  $e^{At}X \sim X$  with  $A \neq 0$ , it follows that  $p(x) = p(e^{At}x)$  for all  $x \in \mathbb{R}^d$ . Since  $e^{At}E_{\Sigma}^{(k)} = E_{\Sigma}^{(k)}$ , the probability distribution of  $X$  must be constant within each ellipsoid  $E_{\Sigma}^{(k)}$ . Since  $\Sigma \succ 0$ , then each set  $E_{\Sigma}^{(k)}$  is non-degenerate in  $\mathbb{R}^d$ , thus inducing a probability density function on  $X$ .  $\blacksquare$

**Lemma 13** Let  $X$  be a  $d$  dimensional r.v. such that  $\dim(\text{span}(X)) < d$  with probability 1. Then,

$$e^{At}X \sim X$$

admits a non-trivial solution  $A \neq 0$ .

**Proof** We expand

$$e^{At}X = X + \left( \sum_{n=1}^{\infty} \frac{t^n}{n!} A^n \right) X$$

Hence, a sufficient condition for the claim is that  $X$  is in the nullspace of  $A$  with probability 1. Since  $\dim(\text{span}(X)) < d$  a.s., then by the rank-nullity theorem, there exists  $A$  such that  $AX = 0$  a.s.  $\blacksquare$

**Proposition 14** Let  $X_0 \sim p_0$  be a discrete random variable. Then  $X_0$  is not auto-rotationally invariant if and only if the support of  $p_0$  spans  $\mathbb{R}^d$ .

**Proof** Lemma 13 provides the only if direction.

Now, let  $\text{span}(X_0) = \mathbb{R}^d$  a.s. Since  $e^{At}$  represents a continuous transformation, and  $X_0$  is supported on a discrete set of points, which cannot all be mapped to 0 by  $A$ , it follows that the support would shift for each  $t > 0$ . We conclude that  $e^{At}X_0 \not\sim X_0$ .  $\blacksquare$

## Appendix B. Additional proofs

**Lemma 15** Let  $\Sigma \succeq 0$  be a symmetric positive semidefinite matrix and suppose that  $A$  is skew-symmetric with respect to  $\Sigma$ , i.e.

$$A\Sigma + \Sigma A^{\top} = 0,$$

then without loss of generality, we may define  $A$  with  $\text{Tr}(A) = 0$ .

**Proof**

$$\text{Tr}(A\Sigma + \Sigma A^{\top}) = \text{Tr}(0) = 0.$$

Using the linearity of the trace and the cyclic property  $\text{Tr}(XY) = \text{Tr}(YX)$ :

$$\begin{aligned} \text{Tr}(A\Sigma + \Sigma A^{\top}) &= \text{Tr}(A\Sigma) + \text{Tr}(A^{\top}\Sigma) \\ &= \text{Tr}(A\Sigma) + \text{Tr}(\Sigma A) \\ &= 2\text{Tr}(A\Sigma). \end{aligned}$$

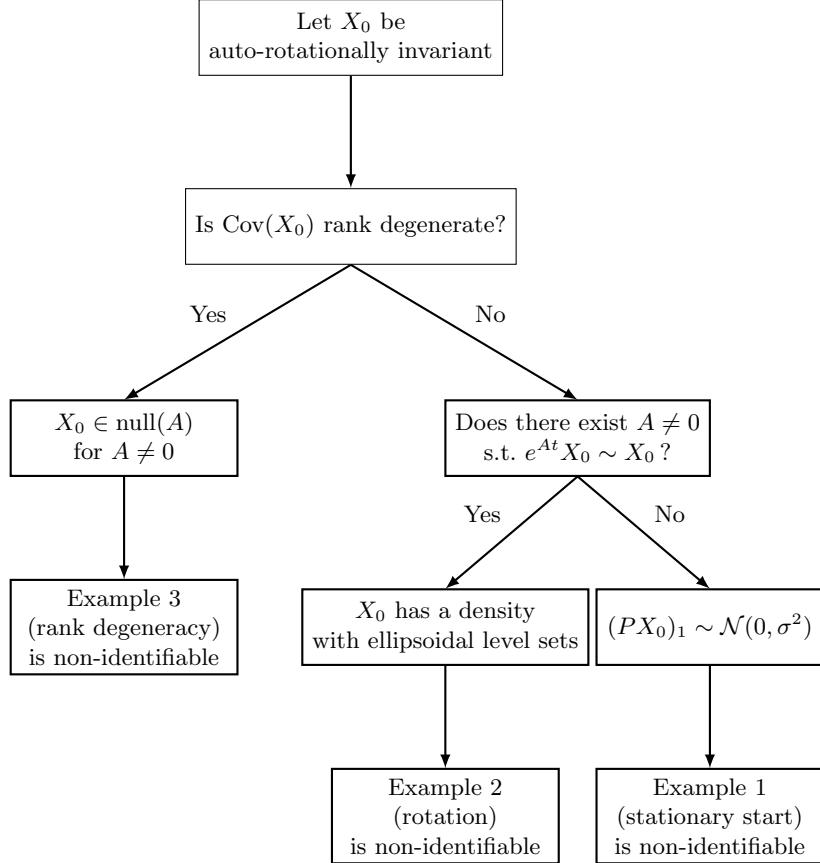


Figure 8: The three types of auto-rotational invariance is illustrated. Each type leads to non-identifiability from marginals, when initialized at the distribution.

Therefore,

$$2\text{Tr}(A\Sigma) = 0 \Rightarrow \text{Tr}(A\Sigma) = 0.$$

If  $\Sigma \succ 0$ , then we immediately conclude  $\text{Tr}(A) = 0$ . Otherwise, we may pick  $A$  such that  $\Sigma_{i,i} = 0 \Rightarrow A_{i,i} = 0$  to ensure that  $\text{Tr}(A) = 0$ . ■

**Corollary 16** *If  $A$  is skew-symmetric with respect to  $\Sigma$ , and  $\Sigma \succ 0$ , then  $Ax$  is a divergence-free vector field:*

$$\nabla \cdot Ax = 0$$

**Proof** We know that

$$\begin{aligned}
 \nabla \cdot Ax &= \sum_{i=1}^d \frac{\partial}{\partial x_i} (A_i x) \\
 &= \sum_{i=1}^d \frac{\partial}{\partial x_i} \sum_{j=1}^d (A_{i,j} x_j) \\
 &= \sum_{i=1}^d A_{i,i} = \text{Tr}(A),
 \end{aligned}$$

which is 0 by Lemma 15. ■

**Proposition 17** *Let  $A \neq 0$  such that  $e^{At}X \sim X$  and let  $H = GG^\top$  satisfy  $AH + HA^\top = 0$ . Then, for all  $\gamma \in \mathbb{R}$ , the SDEs*

$$dX_t = \gamma GdW_t \quad X_0 \sim X \quad (41)$$

$$dY_t = AY_t dt + \gamma GdW_t \quad Y_0 \sim X \quad (42)$$

will have the same marginals  $X_t \sim Y_t \ \forall t \geq 0$ .

**Proof** Intuitively,  $A$  induces a  $\Sigma$ -generalized rotation that is non-identifiable from  $X_0$ , where  $\Sigma = \text{Cov}(X_0)$ . We may directly check that  $X_t \sim Y_t$  for all  $t \geq 0$  by comparing their solutions:

$$\begin{aligned} X_t &= X_0 + \gamma \int_0^t GdW_s = X_0 + \gamma GW_t \sim X_0 + \mathcal{N}(0, \gamma^2 Ht) \\ Y_t &= e^{At}X_0 + \gamma \int_0^t e^{A(t-s)}GdW_s \sim X_0 + \mathcal{N}(0, \gamma^2 \Sigma_t), \end{aligned}$$

where  $\Sigma_t = \int_0^t e^{A(t-s)}He^{A^\top(t-s)}ds$ . Indeed, the fact that the Ito integral,  $\int_0^t e^{A(t-s)}GdW_s$ , is Gaussian, follows from (Oksendal, 2013)[Theorem A.7], since the integrand is deterministic. Then, the fact that it has mean 0 and covariance  $\Sigma_t$  respectively follow from the non-anticipating property and Ito's isometry.

Then, since  $AH + HA^\top = 0$  holds by assumption, we may show that  $\Sigma_t = Ht$ . Indeed, let  $\tau = t - s$  and let  $M(\tau) = e^{A\tau}He^{A^\top\tau}$ . Then,

$$\frac{d}{d\tau}M(\tau) = Ae^{A\tau}He^{A^\top\tau} + e^{A\tau}He^{A^\top\tau}A^\top \quad (43)$$

$$= e^{A\tau}AHe^{A^\top\tau} + e^{A\tau}HA^\top e^{A^\top\tau} \quad (44)$$

$$= e^{A\tau}(AH + HA^\top)e^{A^\top\tau} = 0. \quad (45)$$

Since  $M(0) = H$ , then  $M(\tau) = H$  for all  $\tau$ , and  $\int_0^t e^{A(t-s)}He^{A^\top(t-s)}ds = \int_0^t M(\tau)dt = \int_0^t H = Ht$ , as desired. Thus,

$$Y_t \sim X_0 + \mathcal{N}(0, \Sigma_t) = X_0 + \mathcal{N}(0, \sigma^2 Ht) \sim X_t.$$

This follows from the fact that if  $A_1 \sim A_2$ ,  $B_1 \sim B_2$ ,  $A_1 \perp\!\!\!\perp B_1$ , and  $A_2 \perp\!\!\!\perp B_2$ , then  $A_1 + B_1 \sim A_2 + B_2$ . Indeed, the Gaussian Ito integrals are equal in distribution and independent of  $X_0$ . ■

## Appendix C. SDEs and causality

Let  $V$  be a set of  $d$  endogenous variables  $\{X^{(1)}, X^{(d)}\}$  and  $W$  be a set of exogenous variables  $\{X^{(d+1)}, X^{(d+r)}\}$ , which are excluded from the principal model, but may influence the endogenous variables. Suppose that all variables evolve according to a general SDE, which can be written in “integrand-integrator” form

$$dX_t = a(t, X_t) dh(t, X_t). \quad (46)$$

By integrating and considering each variable  $X_t^{(j)}$  in the endogenous set  $j \in V$ , Boeken and Mooij (2024) showed that we can define a dynamic structural causal model (DSCM) [Definition 1]:

$$X_t^{(j)} = X_0^{(j)} + \int_0^t a_j(s, X_s^{\alpha(j)}) dh_j(s, X_s^{\beta(j)}), \quad (47)$$

where  $\alpha(j), \beta(j) \subset V \cup W$  represent the variables that are used as arguments for  $a_j(t, X_t)$  and  $h_j(t, X_t)$  respectively. In particular, (47) defines a causal graph  $\mathcal{G}$  with vertices  $V \cup W$ , and edges  $E = \{i \rightarrow j : j \in V, i \in \alpha(j) \cup \beta(j)\}$  (Boeken and Mooij, 2024)[Definition 2]. In other words, we only consider edges that point towards variables in the endogenous set, and we include the edge  $i \rightarrow j$  if  $X^{(i)}$  influences the evolution of endogenous variable  $X^{(j)}$  through the integrand  $a_j(t, X_t)$  or integrator  $h_j(t, X_t)$ . Additionally, in Boeken and Mooij (2024), self-loops  $j \rightarrow j$  are excluded to have a simple SCM, but we do not follow this convention in this paper. Under this more general framework, we see that latent confounders can affect endogenous variables via the integrand or integrator, which can be decoupled as drift and diffusion. For instance, any SDE driven by Brownian motion

$$dX_t = b(t, X_t) dt + \sigma(t, X_t) dW_t, \quad (48)$$

can be rewritten in the form (46) by setting  $a(t, X_t) = [b(t, X_t) \ \sigma(t, X_t)]$  and  $h(t, X_t) = [t \ W_t]^\top$ . Given that  $X_t \in \mathbb{R}^d$ ,  $W_t \in \mathbb{R}^m$ , we have corresponding dimensions  $b(X_t) \in \mathbb{R}^d$ ,  $\sigma(X_t) \in \mathbb{R}^{d \times m}$ ,  $Z_t \in \mathbb{R}^{m+1}$ , and  $a(X_t) \in \mathbb{R}^{d \times (m+1)}$ . The DSCM can therefore also be written as

$$X_t^{(j)} = X_0^{(j)} + \int_0^t b_j(s, X_s^{\alpha(j)}) ds + \int_0^t \sigma(s, X_s^{\beta(j)}) dW_s. \quad (49)$$

Under the assumption of independent driving noise, also known as independent integrators (Boeken and Mooij, 2024)[Theorem 4], DSCMs observe graphical Markov properties under local independence (Didelez, 2008; Mogensen and Hansen, 2020, 2022). This is formally defined as  $\beta(j) \subset W$  and  $\beta(i) \cap \beta(j) = \emptyset$  for all  $i, j \in V$ .

Although the observational diffusion  $H = GG^\top$  informs the presence of latent confounders between pairs of variables, we note that it is impossible for  $H$  alone to determine general multidirected edges  $(i_1, \dots, i_p)$  over  $p > 2$  components, which indicate an unobserved confounder of  $X_t^{(i_1)}, \dots, X_t^{(i_p)}$ . Indeed, given only  $H = GG^\top$ , multiple causal interpretations may be possible, because structurally different matrices  $G, \tilde{G}$  can obey  $H = GG^\top = \tilde{G}\tilde{G}^\top$ .

**Example 4 (Non-identifiability of higher order multidirected edges)** Consider two matrices  $G_1, G_2$ , which share the same observational diffusion  $H$ :

$$G_1 = \begin{bmatrix} 0 & 1 & 1 \\ 1 & 0 & 1 \\ 1 & 1 & 0 \end{bmatrix}, \quad G_2 = \begin{bmatrix} \frac{4}{3} & \frac{1}{3} & \frac{1}{3} \\ \frac{1}{3} & \frac{4}{3} & \frac{1}{3} \\ \frac{1}{3} & \frac{1}{3} & \frac{4}{3} \end{bmatrix}, \quad H = G_1 G_1^\top = G_2 G_2^\top = \begin{bmatrix} 2 & 1 & 1 \\ 1 & 2 & 1 \\ 1 & 1 & 2 \end{bmatrix}$$

Given  $G_1$  as the additive noise of an SDE, each pair of variables shares a noise source, since each row shares a nonzero column entry with another row. However, there is no common noise source that is shared among all 3 variables, since each column contains a 0. Hence, the causal interpretation under  $G_1$  consists in three bidirected edges  $1 \leftrightarrow 2$ ,  $1 \leftrightarrow 3$ ,  $2 \leftrightarrow 3$ . In contrast, the causal interpretation under  $G_2$  consists in a single multidirected edge  $(1, 2, 3)$ , since all components share noise sources.

Since  $G_1$  and  $G_2$  admit different causal graphs, despite having the same observational diffusion  $H$ , this shows that  $H$  provides information about the existence of unobserved confounders between pairs of variables, but cannot provide further causal structure about the confounder with respect to the other endogenous variables  $[d] \setminus \{i, j\}$ .

We note that if the noise is not additive, then this further complicates the causal interpretation. In this case, the driving noise  $\sigma(X_t)$  may be a function of the endogenous variables, i.e.  $\beta(j) \cap V \neq \emptyset$ . Thus, unlike the additive noise setting in Theorem 5, simple edges  $i \rightarrow j$  may be informed by the driving noise, via  $\beta(j)$ , rather than just the drift, via  $\alpha(j)$ . However, since only  $\sigma(X_t)\sigma(X_t)^\top$  is observable rather than  $\sigma(X_t)$  itself, observational data under such a model would lend itself to multiple interpretations of the causal graph. The idea is similar to Example 4, where we saw one interpretation feature three bidirected edges and another feature a multi-edge, but under non-additive noise, the ambiguity extends to simple edges  $i \rightarrow j$ . This is illustrated in Example 5.5 in Hansen and Sokol (2014).

The causal framework also highlights the impracticality of common model assumptions within the scRNA-seq literature, namely isotropic diffusion  $H = GG^\top = \sigma^2 I_d$  and irrotational drift  $b(X_t) = \nabla\psi$ . We have seen in Lemma 5 that latent confounders from shared noise can only be modeled with anisotropic diffusion. Moreover, while we expect GRNs to contain feedback loops, i.e. cycles in  $\mathcal{G}$ , imposing irrotational drift prevents most cycles from being considered. Lemma 18 shows that imposing irrotationality on a linear model is equivalent to imposing a symmetric drift, which determines a symmetric causal graph. However, as illustrated in Weinreb et al. (2018)[Fig. 6], symmetric GRNs cannot capture important relationships, such as negative feedback loops or repressilator dynamics. Indeed, consider the 2-cycle  $i \leftrightarrow j$ . By Lemma 5,  $i \rightarrow j$  if  $A_{j,i} \neq 0$  and  $j \rightarrow i$  if  $A_{i,j} \neq 0$ . However, if the model is irrotational, then by Proposition 18,  $A_{i,j} = A_{j,i}$ , which can only model a positive feedback loop.

**Lemma 18** *Let  $X_t$  evolve according to a linear additive noise SDE (3). Then, the drift  $AX_t$  is irrotational if and only if  $A$  is symmetric, i.e.  $A = A^\top$ .*

**Proof** First, we note that for any symmetric matrix  $A$ , the vector field  $Ax$  can be expressed as the gradient of the scalar potential given by the quadratic form  $\phi(x) = x^\top Ax/2$  (Petersen et al., 2008)[(96)-(97)]. Hence,  $Ax$  is irrotational if  $A = A^\top$ .

For the opposite direction, we recall the fact that any gradient field from  $\mathbb{R}^n \rightarrow \mathbb{R}^n$  has a symmetric Jacobian (Williamson and Trotter, 1974; Campbell, 2014). Since the Jacobian of a linear vector field  $Ax : \mathbb{R}^n \rightarrow \mathbb{R}^n$  is  $A$ , we conclude that all irrotational linear vector fields from  $\mathbb{R}^n \rightarrow \mathbb{R}^n$  are given by symmetric matrices.  $\blacksquare$

## Appendix D. Entropy-regularized Optimal Transport

The entropy-regularized optimal transport problem also admits a dual formulation, in terms of finding a pair of potentials  $(f, g)$  with respect to the Gaussian transition kernel  $K(x, y) \propto e^{\frac{c(x, y)}{\epsilon^2}} \propto e^{\frac{-\|y-x\|^2}{2\epsilon^2}}$  (Janati, 2021; Nutz, 2021):

$$\pi^*(x, y) = e^{f^*(x) + g^*(y)} K(x, y) d\mu(x) d\nu(y) \quad (50)$$

$$f^*, g^* = \sup_{f \in \mathcal{L}^1(\mu), g \in \mathcal{L}^1(\nu)} \mathbb{E}_\mu(f) + \mathbb{E}_\nu(g) - \left( \int_{\mathbb{R}^d \times \mathbb{R}^d} e^{f(x) + g(y)} K(x, y) d\mu(x) d\nu(y) - 1 \right). \quad (51)$$

In particular, given marginals  $\mu, \nu$  and the transition kernel  $K$ , Sinkhorn's algorithm uses the dual formulation (51) to find the  $\epsilon$ -entropy regularized optimal transport solution  $\pi^*$ , by solving for  $f^*, g^*$  via iterative projections (Peyré et al., 2019).

**Definition 19 (Markov concatenation of couplings)** *Given Polish spaces  $X_1, X_2, X_3$  and couplings  $\pi_{1,2} \in \mathcal{P}(X_1 \times X_2)$  and  $\pi_{2,3} \in \mathcal{P}(X_2 \times X_3)$  with identical marginals  $\mu_2$  on  $X_2$ , the Markov concatenation  $\pi_{1,2} \circ \pi_{2,3}$  of  $\pi_{1,2}$  and  $\pi_{1,3}$  is a multi-coupling in  $\mathcal{P}(X_1 \times X_2 \times X_3)$  given by*

$$\pi_{1,2} \circ \pi_{2,3}(dx_1, dx_2, dx_3) = \pi_{1,2}(dx_1 | x_2) \mu_2(dx_2) \pi_{2,3}(dx_3 | x_2).$$

Here  $\pi_{12}(dx_1 | x_2)$  is the disintegration of  $\pi_{12}$  with respect to  $\mu_2$  and  $\pi_{2,3}(dx_3 | x_2)$  is the disintegration of  $\pi_{2,3}$  with respect to  $\mu_2$ .

The interpretation of the Markov concatenation is as follows: a random “trajectory” according  $\pi_{12} \circ \pi_{23}$  corresponds to taking the first two steps distributed according to  $\pi_{12}$ , then the third step distributed according to “ $\pi_{23}$  conditional on the second marginal of  $\pi_{12}$ ”. The existence of the Markov concatenation is guaranteed by the disintegration theorem, and Markov concatenations appear naturally in the time-discretized version of trajectory inference via Schrodinger bridges (Lavenant et al., 2021). In particular, given Polish spaces  $X_1, \dots, X_4$  and couplings  $\pi_{12}, \pi_{23}, \pi_{34}$ , it holds that Markov concatenation is associative, and so we can unambiguously define the iterated Markov concatenation  $\pi_{12} \circ \pi_{23} \circ \pi_{34}$  (see Benamou et al. (2019) Section 3.2).

**Proposition 20 (Optimality of anisotropic entropy-regularized optimal transport)** *Let the reference SDE be a linear additive noise SDE with drift  $A$  and diffusion  $H$  (3). Given a set of marginals  $p_0, \dots, p_{N-1}$  over times  $\{t_i\}_{i=0}^{N-1}$  (not necessarily coming from the reference SDE) for which  $D_{KL}(p_i | Leb) < \infty$  for all  $1 \leq i \leq N-1$ , and  $D_{KL}(p_i | (p_{A,H})_i) < \infty$  for all  $1 \leq i \leq N-2$ , suppose there exists  $\pi_{i,i+1}$ , the anisotropic entropic OT solution (23) obtained by Sinkhorn’s algorithm with marginals  $\mu = p_i, \nu = p_{i+1}$  and transition kernel*

$$K_{A,H}^i(x, y) \propto \exp\left(-\frac{1}{2}(y - e^{A(t_{i+1}-t_i)}x)^\top (\Sigma_i)^{-1}(y - e^{A(t_{i+1}-t_i)}x)\right) \quad (52)$$

where  $\Sigma_i = \int_{t_i}^{t_{i+1}} e^{A(t_{i+1}-s)} H e^{A^\top(t_{i+1}-s)} ds$ . Let  $\pi$  denote the joint distribution given by the Markov concatenation of couplings (see Definition 19):

$$\pi = \pi_{0,1} \circ \dots \circ \pi_{N-2,N-1},$$

Then,  $\pi$  minimizes relative entropy to the law of the reference SDE:

$$\pi = \arg \min_{\pi \in \Pi(p_0, \dots, p_{N-1})} D_{KL}(\pi \| p_{A,H}^N),$$

where  $p_{A,H}^N$  is the law of the reference SDE, discretized over time points  $t_0, \dots, t_{N-1}$ .

**Proof** For each  $i = 0, \dots, N-1$ , by (5), we have  $\pi_i = \arg \min_{\pi \in \Pi(p_i, p_{i+1})} D_{KL}(\pi \| K_{A,H}^i)$ . Since  $K_{A,H}^i \sim \mathcal{N}(e^{A(t_{i+1}-t_i)} X_t, \Sigma_i)$  is the transition kernel of the SDE at time  $t_i$  (Särkkä and Solin, 2019)[Sec 6.1], this implies that

$$\pi_i = \arg \min_{\pi \in \Pi(p_i, p_{i+1})} D_{KL}(\pi \| (p_{A,H})_{i,i+1}),$$

where  $(p_{A,H})_{i,i+1}$  denotes the joint distribution of  $p_{A,H}$  at the two time points  $t_i, t_{i+1}$ . The details are as follows. Let  $K_{i,i+1}(x, y)$  denote the transition kernel from time  $t_i$  to time  $t_{i+1}$  for the SDE  $dX_t = AX_t + GdW_t$ . In particular, if  $(p_{A,H})_i$  is the marginal of this SDE at time  $t_i$ , then we have that  $K_{i,i+1}(x, y)d(p_{A,H})_i(x)dy$  is equal to the joint distribution  $(p_{A,H})_{i,i+1}$ . Hence

$$D_{KL}(\pi | (p_{A,H})_{i,i+1}) = D_{KL}(\pi | K_{A,H}(x, y)d(p_{A,H})_i(x)dy).$$

We claim that for any  $\pi \in \Pi(p_i, p_{i+1})$ ,

$$D_{KL}(\pi | K_{A,H}(x, y)d(p_{A,H})_i dy) = D_{KL}(\pi | K_{A,H}(x, y)dp_i(x)dp_{i+1}(y)) + D_{KL}(p_i | (p_{A,H})_i) + D_{KL}(p_{i+1} | Leb).$$

Indeed,

$$\begin{aligned}
D_{KL}(\pi \mid K_{A,H}(x, y) d(p_{A,H})_i dy) &= \int \log \left( \frac{d\pi}{d(K \cdot (p_{A,H})_i \otimes \text{Leb})}(x, y) \right) d\pi \\
&= \int \log \left( \frac{d\pi}{d(K \cdot p_i \otimes dp_{i+1})}(x, y) \frac{d(K \cdot p_i \otimes dp_{i+1})}{d(K \cdot (p_{A,H})_i \otimes \text{Leb})}(x, y) \right) d\pi \\
&= \int \log \left( \frac{d\pi}{d(K \cdot p_i \otimes dp_{i+1})}(x, y) \frac{dp_i}{d(p_{A,H})_i}(x) \frac{dp_{i+1}}{d\text{Leb}}(y) \right) d\pi \\
&= D_{KL}(\pi \mid K_{A,H}(x, y) dp_i(x) dp_{i+1}(y)) + D_{KL}(p_i \mid (p_{A,H})_i) + D_{KL}(p_{i+1} \mid \text{Leb}).
\end{aligned}$$

Note that  $(p_{A,H})_0 = p_0$ . Hence, under the assumption that for all  $i = 1, \dots, N-1$ ,  $D_{KL}(p_{i+1} \mid \text{Leb}) < \infty$ , the minimizers for the following two minimization problems are identical:

$$\min_{\pi \in \Pi(p_i p_{i+1})} D_{KL}(\pi \mid (p_{A,H})_{i,i+1}) \text{ and } \min_{\pi \in \Pi(p_i p_{i+1})} D_{KL}(\pi \mid K_{A,H}(x, y) dp_i(x) dp_{i+1}(y)).$$

Since  $\pi$  is constructed as a Markov concatenation, the conclusion follows from Lemma 3.4 of Benamou et al. (2019), which in this case tells us that: if  $p_{A,H}^N$  is the projection of the law of the SDE onto the set of times  $\{t_0, \dots, t_{N-1}\}$ , then for any  $N$ -coupling  $\pi$  which is constructed as a Markovian concatenation  $\pi_{0,1} \circ \dots \pi_{N-2,N-1}$ , and has  $i$ th marginal equal to  $p_i$ , we have

$$D_{KL}(\pi \mid p_{A,H}^N) = \sum_{i=0}^{N-2} D_{KL}(\pi_i \mid (p_{A,H})_{i,i+1}) - \sum_{i=1}^{N-2} D_{KL}(p_i \mid (p_{A,H})_i).$$

Hence minimizing over each  $D_{KL}(\pi_{i,i+1} \mid (p_{A,H})_{i,i+1})$  (for  $\pi \in \Pi(p_i, p_{i+1})$ ) is equivalent to minimizing over Markovian  $\pi$ 's with  $i$ th marginal  $p_i$ . ■

The previous proposition assumes that  $D_{KL}(p_i \mid \text{Leb}) < \infty$  for all  $i \neq 0$ . The following brief computation shows that this assumption is satisfied in the case where the diffusion matrix is non-degenerate.

We note that  $X_t \sim e^{At} X_0 + \int_0^t e^{A(t-s)} G dW_s$ . As  $X_0$  is independent from the Brownian noise  $W_s$ , and  $\int_0^t e^{A(t-s)} G dW_s \sim \mathcal{N}(0, \Sigma_t)$ , where  $\Sigma_t = \int_0^t e^{A(t-s)} H e^{A^\top(t-s)} ds$ , it follows that

$$p_t = p_0 * \mathcal{N}(0, \Sigma_t).$$

Thus, we may compute (Cover, 1999, Theorem 9.4.1)

$$D_{KL}(\mathcal{N}(0, \Sigma_t) \mid \text{Leb}) = \frac{1}{2} \log(2\pi e)^d \det(\Sigma_t).$$

From the definition of  $\Sigma_t$ , we note that  $\det(\Sigma_t) \neq 0$  as long as  $H = GG^\top$  is full rank. Then, we use the fact that the  $D_{KL}(\cdot \mid \text{Leb})$  is convex, and apply Jensen's inequality for measures, to deduce that

$$D_{KL}(p_0 * \mathcal{N}(0, \Sigma_t) \mid \text{Leb}) \leq \int D_{KL}(\mathcal{N}(x, \Sigma_t) \mid \text{Leb}) dp_0(x) = D_{KL}(\mathcal{N}(0, \Sigma_t) \mid \text{Leb}).$$

This shows directly that  $p_t$  has finite entropy whenever  $t > 0$  as desired.

**Remark 21 (Applying EOT for SDE trajectory inference)** *In the standard  $\epsilon$ -regularized OT problem (22), the cost is the squared Euclidean distance, and  $K \sim \mathcal{N}(x, \epsilon^2 \mathbf{I}_d)$  is an isotropic Gaussian kernel. As noted in Lavenant et al. (2021), this implies that entropy regularized OT can*

be leveraged for trajectory inference from observed marginals, given a reference SDE. For example, to find the discretized law on paths  $\pi^* \in \Pi(\mu, \nu)$  satisfying  $P(X_t = \mu, X_{t+\Delta t} = \nu)$ , which minimizes relative entropy to the law of a pure diffusion process  $dX_t = \sigma dW_t$ , one should set the entropic regularization  $\epsilon^2 = \sigma^2 \Delta t$ . This would correspond to minimizing the KL divergence to  $K(x, y) = e^{-\frac{\|y-x\|^2}{2\sigma^2 \Delta t}} \sim \mathcal{N}(x, \sigma^2 \Delta t)$ , which is the transition kernel of the reference SDE. Similarly, as done in Zhang (2024), one can perform trajectory inference given an Ornstein-Uhlenbeck reference SDE  $dX_t = -AX_t dt + \sigma dW_t$  by approximating the transition distribution  $X_{t+\Delta t|t}$  via  $K(x, y) = e^{-\frac{\|y-e^{A\Delta t}x\|^2}{2\sigma^2 \Delta t}}$ . This would correspond to reweighting the squared Euclidean cost with the drift matrix  $A$ , such that  $c(x, y) = \|y - e^{A\Delta t}x\|/2$ , and applying standard entropy regularized OT with  $\epsilon^2 = \sigma^2 \Delta t$ .

## Appendix E. Maximum Likelihood Estimation

**Proof** [Proof of Proposition (7)] We follow the standard procedure for deriving maximum likelihood estimators (Peiris et al., 2003; Pavliotis, 2014). Our likelihood function is given by

$$\mathcal{L} = \prod_{i=0}^{N-2} \left( \prod_{j=0}^{M-1} p(X_{i+1}^{(j)} | X_i^{(j)}) \right),$$

where we have denoted  $X_i = X_{t_i}$  for shorthand. As in Pavliotis (2014), we consider the discretized law  $X_{i+1}|X_i \sim \mathcal{N}(X_i + AX_i \Delta t, H \Delta t)$ , which implies

$$p(X_{i+1}|X_i) = \frac{1}{(2\pi \Delta t)^{d/2} \det(H)^{1/2}} \exp \left( -\frac{1}{2} (\Delta X_i^{(j)} - AX_i^{(j)} \Delta t)^\top (H \Delta t)^{-1} (\Delta X_i^{(j)} - AX_i^{(j)} \Delta t) \right),$$

where  $\Delta X_i^{(j)} = X_{i+1}^{(j)} - X_i^{(j)}$ . Plugging this back into the likelihood expression yields

$$\mathcal{L} = \frac{1}{(2\pi \Delta t)^{\frac{dM(N-1)}{2}} \det(H)^{\frac{M(N-1)}{2}}} \exp \left( - \sum_{i=0}^{N-2} \sum_{j=0}^{M-1} \frac{1}{2} (\Delta X_i^{(j)} - AX_i^{(j)} \Delta t)^\top (H \Delta t)^{-1} (\Delta X_i^{(j)} - AX_i^{(j)} \Delta t) \right) \quad (53)$$

$$\log(\mathcal{L}) = -\frac{M(N-1)}{2} (d \log(2\pi \Delta t) + \log(\det(H))) - \frac{1}{2} \sum_{i=0}^{N-2} \sum_{j=0}^{M-1} (\Delta X_i^{(j)} - AX_i^{(j)} \Delta t)^\top (H \Delta t)^{-1} (\Delta X_i^{(j)} - AX_i^{(j)} \Delta t) \quad (54)$$

We then derive the maximum likelihood estimators through matrix calculus (Petersen et al., 2008):

$$\begin{aligned} \frac{d \log(\mathcal{L})}{dA} &= -\frac{1}{2} \sum_{i=0}^{N-2} \sum_{j=0}^{M-1} \frac{d}{dA} (\Delta X_i^{(j)} - AX_i^{(j)} \Delta t)^\top (H \Delta t)^{-1} (\Delta X_i^{(j)} - AX_i^{(j)} \Delta t) \\ &= -\frac{1}{2} \sum_{i=0}^{N-2} \sum_{j=0}^{M-1} -2\Delta t \frac{d}{dA} ((\Delta X_i^{(j)})^\top (H \Delta t)^{-1} AX_i^{(j)}) + \Delta t^2 \frac{d}{dA} (X_i^{(j)\top} A^\top (H \Delta t)^{-1} AX_i^{(j)}) \\ &= -\frac{1}{2} \sum_{i=0}^{N-2} \sum_{j=0}^{M-1} -2\Delta t (H \Delta t)^{-1} (\Delta X_i^{(j)}) X_i^{(j)\top} + 2\Delta t^2 (H \Delta t)^{-1} AX_i^{(j)} X_i^{(j)\top} \\ &= \sum_{i=0}^{N-2} \sum_{j=0}^{M-1} (H)^{-1} (\Delta X_i^{(j)}) X_i^{(j)\top} - \Delta t (H)^{-1} AX_i^{(j)} X_i^{(j)\top} \end{aligned}$$

We can solve for the MLE linear drift  $A$  by setting  $\frac{d\log(\mathcal{L})}{dA} = 0$ :

$$\begin{aligned} \sum_{i=0}^{N-2} \sum_{j=0}^{M-1} \Delta t(H)^{-1} A X_i^{(j)} X_i^{(j)\top} &= \sum_{i=0}^{N-2} \sum_{j=0}^{M-1} (H)^{-1} (\Delta X_i^{(j)}) X_i^{(j)\top} \\ \Delta t(H)^{-1} A \sum_{i=0}^{N-2} \sum_{j=0}^{M-1} X_i^{(j)} X_i^{(j)\top} &= (H)^{-1} \sum_{i=0}^{N-2} \sum_{j=0}^{M-1} \Delta X_i^{(j)} X_i^{(j)\top} \\ A &= \frac{1}{\Delta t} \left( \sum_{i=0}^{N-2} \sum_{j=0}^{M-1} \Delta X_i^{(j)} X_i^{(j)\top} \right) \left( \sum_{i=0}^{N-2} \sum_{j=0}^{M-1} X_i^{(j)} X_i^{(j)\top} \right)^{-1} \end{aligned}$$

We now estimate the diffusion  $H$ . For simplicity, we work with  $H^{-1} = (GG^\top)^{-1}$

$$\begin{aligned} \frac{d\log(L)}{dH^{-1}} &= \frac{d}{dH^{-1}} \left( \frac{M(N-1)}{2} \log(\det(H^{-1})) - \frac{1}{2\Delta t} \sum_{i=0}^{N-2} \sum_{j=0}^{M-1} (\Delta X_i^{(j)} - AX_i^{(j)}\Delta t)^\top H^{-1} (\Delta X_i^{(j)} - AX_i^{(j)}\Delta t) \right) \\ &= \frac{M(N-1)}{2} H - \frac{1}{2\Delta t} \sum_{i=0}^{N-2} \sum_{j=0}^{M-1} (\Delta X_i^{(j)} - AX_i^{(j)}\Delta t) (\Delta X_i^{(j)} - AX_i^{(j)}\Delta t)^\top \end{aligned}$$

We can solve for the MLE additive noise  $H$  by setting  $\frac{d\log(\mathcal{L})}{dH^{-1}} = 0$

$$\begin{aligned} H &= \frac{1}{M(N-1)\Delta t} \sum_{i=0}^{N-2} \sum_{j=0}^{M-1} (\Delta X_i^{(j)} - AX_i^{(j)}\Delta t) (\Delta X_i^{(j)} - AX_i^{(j)}\Delta t)^\top \\ &= \frac{1}{MT} \sum_{i=0}^{N-2} \sum_{j=0}^{M-1} (\Delta X_i^{(j)} - AX_i^{(j)}\Delta t) (\Delta X_i^{(j)} - AX_i^{(j)}\Delta t)^\top. \end{aligned}$$

■

**Corollary 22** *Let  $X_t$  evolve according to a general additive noise SDE (2). Then the log-likelihood function is given by*

$$\begin{aligned} \mathcal{L} &= \frac{1}{(2\pi\Delta t)^{\frac{dM(N-1)}{2}} \det(H)^{\frac{M(N-1)}{2}}} \exp \left( - \sum_{i=0}^{N-2} \sum_{j=0}^{M-1} \frac{1}{2} (\Delta X_i^{(j)} - b(X_i^{(j)})\Delta t)^\top (H\Delta t)^{-1} (\Delta X_i^{(j)} - b(X_i^{(j)})\Delta t) \right) \\ \log(\mathcal{L}) &= -\frac{M(N-1)}{2} (d\log(2\pi\Delta t) + \log(\det(H))) - \frac{1}{2} \sum_{i=0}^{N-2} \sum_{j=0}^{M-1} (\Delta X_i^{(j)} - b(X_i^{(j)})\Delta t)^\top (H\Delta t)^{-1} (\Delta X_i^{(j)} - b(X_i^{(j)})\Delta t) \end{aligned}$$

Hence, given that the drift function  $b$  is parameterized by values  $\alpha_b^{(k)}$ , the maximum likelihood solution for the drift function  $b$  obeys

$$0 = -\frac{1}{2} \sum_{i=0}^{N-2} \sum_{j=0}^{M-1} \frac{d}{d\alpha_b^{(k)}} (\Delta X_i^{(j)} - b(X_i^{(j)})\Delta t)^\top (H\Delta t)^{-1} (\Delta X_i^{(j)} - b(X_i^{(j)})\Delta t)$$

The MLE for the diffusion  $H$  admits the closed solution

$$H = \frac{1}{MT} \sum_{i=0}^{N-1} \sum_{j=0}^{M-1} (\Delta X_i^{(j)} - b(X_i^{(j)})\Delta t) (\Delta X_i^{(j)} - b(X_i^{(j)})\Delta t)^\top.$$

**Proposition 23 (Exact MLE estimators for drift and diffusion of 1 dimensional SDE (3) from multiple trajectory time series)**  
*Given  $M$  different trajectory time series over  $N$  different times:  $\{X_{t_i}^{(j)} : i \in 0, \dots, N-1, j \in 0, \dots, M-1\}$  sampled from the linear additive noise SDE (3), the maximum likelihood solution for linear drift is approximated by*

$$\hat{A} = \frac{1}{\Delta t} \log \left( \frac{\sum_{i=0}^{N-2} \sum_{j=0}^{M-1} X_{i+1}^{(j)} X_i^{(j)}}{\sum_{i=0}^{N-2} \sum_{j=0}^{M-1} X_i^{(j)2}} \right) \quad (55)$$

and the maximum likelihood solution for diffusion is approximated by

$$\hat{\sigma}^2 = \frac{1}{M(N-1)\Delta t} \sum_{i=0}^{N-2} \sum_{j=0}^{M-1} (X_{i+1}^{(j)} - e^{A\Delta t} X_i^{(j)})^2 \quad (56)$$

**Proof** We proceed as in the proof of Proposition (7). The exact log-likelihood for the one dimensional case is

$$\log(\mathcal{L}) = -\frac{M(N-1)}{2} (\log(2\pi\Delta t) + \log(\sigma^2)) - \frac{1}{2\sigma^2\Delta t} \sum_{i=0}^{N-2} \sum_{j=0}^{M-1} (X_{i+1}^{(j)} - e^{A\Delta t} X_i^{(j)})^2$$

To solve for  $\hat{A}$ , we compute

$$\begin{aligned} 0 &= \frac{\partial \log(\mathcal{L})}{\partial A} \propto \sum_{i=0}^{N-2} \sum_{j=0}^{M-1} \frac{\partial}{\partial A} \left( -2X_{i+1}^{(j)} X_i^{(j)} e^{A\Delta t} + e^{2A\Delta t} X_i^{(j)2} \right) \\ e^{2A\Delta t} \sum_{i=0}^{N-2} \sum_{j=0}^{M-1} X_i^{(j)2} &= e^{A\Delta t} \sum_{i=0}^{N-2} \sum_{j=0}^{M-1} X_{i+1}^{(j)} X_i^{(j)} \\ e^{A\Delta t} &= \frac{\sum_{i=0}^{N-2} \sum_{j=0}^{M-1} X_{i+1}^{(j)} X_i^{(j)}}{\sum_{i=0}^{N-2} \sum_{j=0}^{M-1} X_i^{(j)2}} \\ A &= \frac{1}{\Delta t} \log \left( \frac{\sum_{i=0}^{N-2} \sum_{j=0}^{M-1} X_{i+1}^{(j)} X_i^{(j)}}{\sum_{i=0}^{N-2} \sum_{j=0}^{M-1} X_i^{(j)2}} \right) \end{aligned}$$

Similarly, to solve for  $\hat{\sigma}^2$ , we compute

$$\begin{aligned} 0 &= \frac{\partial \log(\mathcal{L})}{\partial \sigma^2} \propto -\frac{M(N-1)}{2\sigma^2} + \frac{1}{2\Delta t} \frac{1}{(\sigma^2)^2} \sum_{i=0}^{N-2} \sum_{j=0}^{M-1} (X_{i+1}^{(j)} - e^{A\Delta t} X_i^{(j)})^2 \\ \frac{M(N-1)}{2} &= \frac{1}{2\Delta t \sigma^2} \sum_{i=0}^{N-2} \sum_{j=0}^{M-1} (X_{i+1}^{(j)} - e^{A\Delta t} X_i^{(j)})^2 \\ \sigma^2 &= \frac{1}{M(N-1)\Delta t} \sum_{i=0}^{N-2} \sum_{j=0}^{M-1} (X_{i+1}^{(j)} - e^{A\Delta t} X_i^{(j)})^2 \end{aligned}$$

■

**Remark 24** Previous works have predominately focused on the case of observing a single long trajectory rather than a collection of short trajectories. Suppose that one observes a set of  $N$  observed trajectories, then drift estimation may also be performed by averaging the classical MLE estimator for a single trajectory across observations:  $\mathbb{E}_N[\hat{A}_T] = \frac{1}{N} \frac{\int_0^T X_t dX_t}{\int_0^T X_t^2 dt}$ . Note that this is distinct from the MLE estimator that we derived for multiple trajectories in (26). Indeed, we observe that the latter estimator converges at a much faster rate than the averaged classical estimator.

## Appendix F. Consistency experiments

We present the results of additional experiments verifying the consistency of our method, as we increase the number of samples  $N$  per marginal.

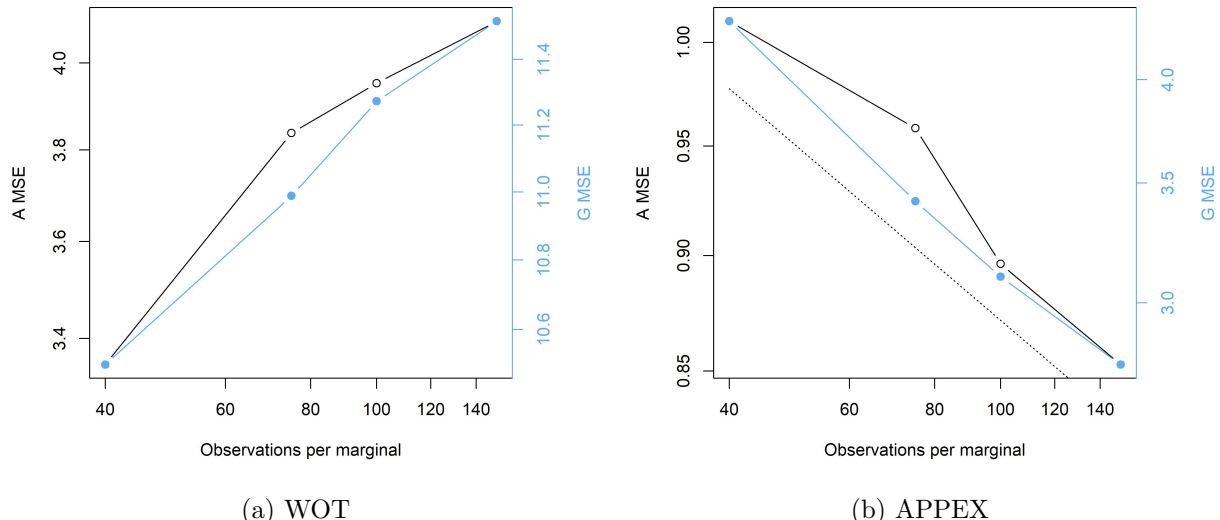


Figure 9: Average mean squared error (MSE) of  $A$  and  $GG^\top$  as the number of observations per marginal increases across 50 random 2d systems. Note that this is a log-log plot and the dotted line in the APPEX plot shows that the convergence follows a power law relationship with exponent  $-0.125$ .

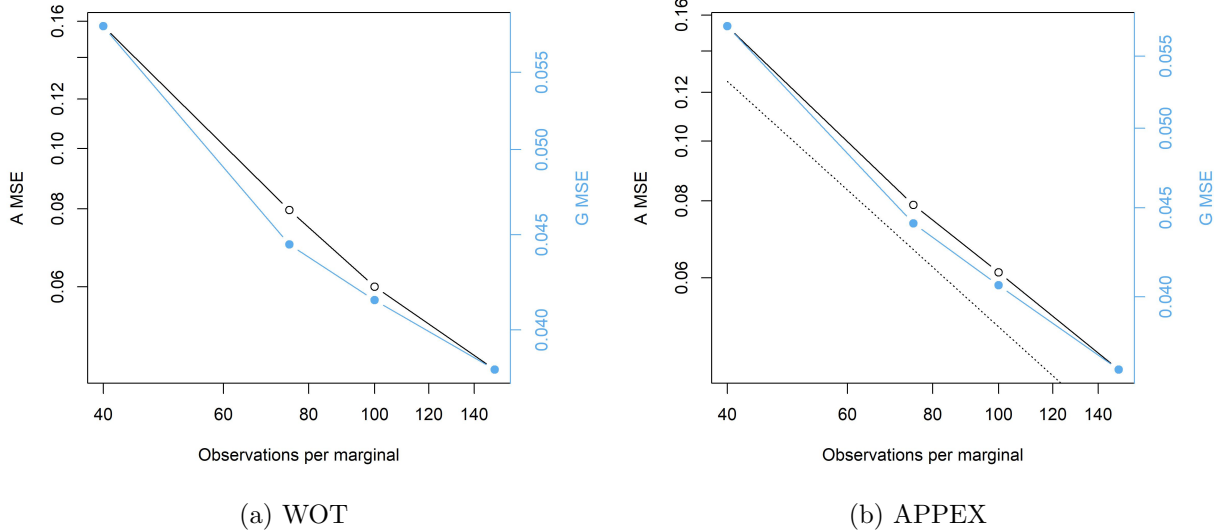


Figure 10: Average mean squared error (MSE) of  $A$  and  $GG^\top$  as the number of observations per marginal increases across 70 random 12d systems. In this log-log plot, the dotted line in the APPEX plot indicates that the convergence follows a power law relationship with exponent  $-1$ .

## Appendix G. Table of notations

Notation	Meaning
$b(X_t)$	Drift function of a general SDE
$A$	Drift matrix of a linear SDE
$G$	Diffusion matrix of an additive noise SDE
$H = GG^\top$	Observational diffusion matrix
$p_t \sim X_t$	Temporal marginal distribution of the SDE at time $t$
$p(x, t)$	Probability density of the process at time $t$ , assuming existence
$X_i = X_{t_i}$	Distribution of SDE at $i$ th observation time
$\Delta X_i$	$X_{i+1} - X_i$
$p_i \sim X_{t_i}$	Temporal marginal distribution of the SDE at measured time $t_i$
$N$	Number of observed temporal marginals
$\hat{p}_i$	Empirical temporal marginal of the SDE at measured time $t_i$
$x_{t_i}^{(j)}$	$j$ th sample from $i$ th empirical marginal
$M_i$	Number of samples for the $i$ th empirical temporal marginal $\hat{p}_i$
$\Sigma$	Covariance of an initial distribution $X_0$
$\epsilon$	Scalar parameter for regularizing entropy-regularized optimal transport (EOT)
$\Sigma(\theta)$	(Possibly) anisotropic matrix parameter for regularizing anisotropic entropy regularized optimal transport (AEOT)

## References

- A. Aalto, L. Viitasaari, P. Ilmonen, L. Mombaerts, and J. Gonçalves. Gene regulatory network inference from sparsely sampled noisy data. *Nature communications*, 11(1):3493, 2020.
- E. E. Adams and L. W. Gelhar. Field study of dispersion in a heterogeneous aquifer: 2. spatial moments analysis. *Water Resources Research*, 28(12):3293–3307, 1992.

H. Akaike. Information theory and an extension of the maximum likelihood principle. In *Selected papers of Hirotugu Akaike*, pages 199–213. Springer, 1998.

J. Altschuler, J. Niles-Weed, and P. Rigollet. Near-linear time approximation algorithms for optimal transport via sinkhorn iteration. *Advances in neural information processing systems*, 30, 2017.

Aristotle. *Generation of Animals*, volume 366 of *Loeb Classical Library*. Harvard University Press, Cambridge, MA, 1942.

L. Atanackovic, A. Tong, B. Wang, L. J. Lee, Y. Bengio, and J. S. Hartford. Dyngfn: Towards bayesian inference of gene regulatory networks with gflownets. *Advances in Neural Information Processing Systems*, 36, 2024.

J.-D. Benamou, G. Carlier, S. Di Marino, and L. Nenna. An entropy minimization approach to second-order variational mean-field games. *Mathematical Models and Methods in Applied Sciences*, 29(08):1553–1583, 2019.

K. J. Beven, D. E. Henderson, and A. D. Reeves. Dispersion parameters for undisturbed partially saturated soil. *Journal of hydrology*, 143(1-2):19–43, 1993.

J. P. Bishwal. *Parameter estimation in stochastic differential equations*. Springer, 2007.

F. Black and M. Scholes. The pricing of options and corporate liabilities. *Journal of political economy*, 81(3):637–654, 1973.

P. Boeken and J. M. Mooij. Dynamic structural causal models. *arXiv preprint arXiv:2406.01161*, 2024.

J. M. Boggs, S. C. Young, L. M. Beard, L. W. Gelhar, K. R. Rehfeldt, and E. E. Adams. Field study of dispersion in a heterogeneous aquifer: 1. overview and site description. *Water Resources Research*, 28(12):3281–3291, 1992.

L. Brogat-Motte, R. Bonalli, and A. Rudi. Learning controlled stochastic differential equations. *arXiv preprint arXiv:2411.01982*, 2024.

P. Brouillard, S. Lachapelle, A. Lacoste, S. Lacoste-Julien, and A. Drouin. Differentiable causal discovery from interventional data. *Advances in Neural Information Processing Systems*, 33: 21865–21877, 2020.

A. G. Cahill, R. Beckie, B. Ladd, E. Sandl, M. Goetz, J. Chao, J. Soares, C. Manning, C. Chopra, N. Finke, et al. Advancing knowledge of gas migration and fugitive gas from energy wells in northeast british columbia, canada. *Greenhouse Gases: Science and Technology*, 9(2):134–151, 2019.

L. Campbell. Reduction theorems for the strong real jacobian conjecture. In *Annales Polonici Mathematici*, volume 110, pages 1–11. Institute of Mathematics Polish Academy of Sciences, 2014.

P. Chakraborty, M. M. Meerschaert, and C. Y. Lim. Parameter estimation for fractional transport: A particle-tracking approach. *Water resources research*, 45(10), 2009.

D. Chen, R. Carsel, L. Moeti, and B. Vona. Assessment and prediction of contaminant transport and migration at a florida superfund site. *Environmental monitoring and assessment*, 57:291–299, 1999.

T. Chen, G.-H. Liu, and E. A. Theodorou. Likelihood training of schrödinger bridge using forward-backward sdes theory. *arXiv preprint arXiv:2110.11291*, 2021.

L. Chizat, S. Zhang, M. Heitz, and G. Schiebinger. Trajectory inference via mean-field langevin in path space. *Advances in Neural Information Processing Systems*, 35:16731–16742, 2022.

M. A. Coomer, L. Ham, and M. P. Stumpf. Noise distorts the epigenetic landscape and shapes cell-fate decisions. *Cell Systems*, 13(1):83–102, 2022.

T. M. Cover. *Elements of information theory*. John Wiley & Sons, 1999.

V. De Bortoli, J. Thornton, J. Heng, and A. Doucet. Diffusion schrödinger bridge with applications to score-based generative modeling. *Advances in Neural Information Processing Systems*, 34: 17695–17709, 2021.

V. Didelez. Graphical models for marked point processes based on local independence. *Journal of the Royal Statistical Society Series B: Statistical Methodology*, 70(1):245–264, 2008.

J. du Buisson and H. Touchette. Dynamical large deviations of linear diffusions. *Physical Review E*, 107(5):054111, 2023.

A. Einstein. *Investigations on the Theory of the Brownian Movement*. Courier Corporation, 1956.

A. M. Elfeki. Prediction of contaminant plumes (shapes, spatial moments and macrodispersion) in aquifers with insufficient geological information. *Journal of Hydraulic Research*, 44(6):841–856, 2006.

W. Fang and M. B. Giles. Adaptive euler–maruyama method for sdes with nonglobally lipschitz drift. *The Annals of Applied Probability*, 30(2):526–560, 2020.

J. A. Farrell, Y. Wang, S. J. Riesenfeld, K. Shekhar, A. Regev, and A. F. Schier. Single-cell reconstruction of developmental trajectories during zebrafish embryogenesis. *Science*, 360(6392): eaar3131, 2018.

A. Forrow. Consistent diffusion matrix estimation from population time series. *arXiv preprint arXiv:2408.14408*, 2024.

E. Frind, J. Molson, and D. Rudolph. Well vulnerability: a quantitative approach for source water protection. *Groundwater*, 44(5):732–742, 2006.

A. Genevay, L. Chizat, F. Bach, M. Cuturi, and G. Peyré. Sample complexity of sinkhorn divergences. In *The 22nd international conference on artificial intelligence and statistics*, pages 1574–1583. PMLR, 2019.

P. Ghosal, M. Nutz, and E. Bernton. Stability of entropic optimal transport and schrödinger bridges. *Journal of Functional Analysis*, 283(9):109622, 2022.

N. Hansen and A. Sokol. Causal interpretation of stochastic differential equations. *Electronic Journal of Probability*, 2014.

T. Hashimoto, D. Gifford, and T. Jaakkola. Learning population-level diffusions with generative rnns. In *International Conference on Machine Learning*, pages 2417–2426. PMLR, 2016.

M. B. Hazas, F. Ziliotto, J. Lee, M. Rolle, and G. Chiogna. Evolution of plume geometry, dilution and reactive mixing in porous media under highly transient flow fields at the surface water-groundwater interface. *Journal of Contaminant Hydrology*, 258:104243, 2023.

M. Holmes-Cerfon. Applied stochastic analysis, 2015.

H. Huang. One-step data-driven generative model via schrödinger bridge. *arXiv preprint arXiv:2405.12453*, 2024.

H. Janati. *Advances in Optimal transport and applications to neuroscience*. PhD thesis, Institut Polytechnique de Paris, 2021.

H. Janati, B. Muzellec, G. Peyré, and M. Cuturi. Entropic optimal transport between unbalanced gaussian measures has a closed form. *Advances in neural information processing systems*, 33: 10468–10479, 2020.

H. Lavenant, S. Zhang, Y.-H. Kim, and G. Schiebinger. Towards a mathematical theory of trajectory inference. *arXiv preprint arXiv:2102.09204*, 2021.

J. Ledolter. Estimation bias in the first-order autoregressive model and its impact on predictions and prediction intervals. *Communications in Statistics-Simulation and Computation*, 38(4):771–787, 2009.

P. C. Lichtner, S. Kelkar, and B. Robinson. New form of dispersion tensor for axisymmetric porous media with implementation in particle tracking. *Water Resources Research*, 38(8):21–1, 2002.

Y. Liu, E. Robeva, and H. Wang. Learning linear non-gaussian graphical models with multidirected edges. *Journal of Causal Inference*, 9(1):250–263, 2021.

L. Locatelli, P. J. Binning, X. Sanchez-Vila, G. L. Søndergaard, L. Rosenberg, and P. L. Bjerg. A simple contaminant fate and transport modelling tool for management and risk assessment of groundwater pollution from contaminated sites. *Journal of contaminant hydrology*, 221:35–49, 2019.

L. Lorch, A. Krause, and B. Schölkopf. Causal modeling with stationary diffusions. In *International Conference on Artificial Intelligence and Statistics*, pages 1927–1935. PMLR, 2024.

L. Lu, P. Jin, G. Pang, Z. Zhang, and G. E. Karniadakis. Learning nonlinear operators via deeponet based on the universal approximation theorem of operators. *Nature machine intelligence*, 3(3): 218–229, 2021.

J. MacInnes and F. Bracco. Stochastic particle dispersion modeling and the tracer-particle limit. *Physics of Fluids A: Fluid Dynamics*, 4(12):2809–2824, 1992.

D. Mackay, D. Freyberg, P. Roberts, and J. Cherry. A natural gradient experiment on solute transport in a sand aquifer: 1. approach and overview of plume movement. *Water Resources Research*, 22(13):2017–2029, 1986.

S. Maddu, V. Chardès, M. Shelley, et al. Inferring biological processes with intrinsic noise from cross-sectional data. *arXiv preprint arXiv:2410.07501*, 2024.

C. Man and C. W. Tsai. Stochastic partial differential equation-based model for suspended sediment transport in surface water flows. *Journal of engineering mechanics*, 133(4):422–430, 2007.

S. Mandt, M. Hoffman, and D. Blei. A variational analysis of stochastic gradient algorithms. In *International conference on machine learning*, pages 354–363. PMLR, 2016.

G. Manten, C. Casolo, E. Ferrucci, S. W. Mogensen, C. Salvi, and N. Kilbertus. Signature kernel conditional independence tests in causal discovery for stochastic processes. *arXiv preprint arXiv:2402.18477*, 2024.

J. Marcinkiewicz. Sur une propriété de la loi de gauss. *Mathematische Zeitschrift*, 44(1):612–618, 1939.

J. C. Maxwell. Ii. illustrations of the dynamical theory of gases. *The London, Edinburgh, and Dublin Philosophical Magazine and Journal of Science*, 20(130):21–37, 1860.

P. McCULLAGH. Tensor notation and cumulants of polynomials. *Biometrika*, 71(3):461–476, 1984.

C. Meng, Y. He, Y. Song, J. Song, J. Wu, J.-Y. Zhu, and S. Ermon. Sdedit: Guided image synthesis and editing with stochastic differential equations. *arXiv preprint arXiv:2108.01073*, 2021.

S. W. Mogensen and N. R. Hansen. Markov equivalence of marginalized local independence graphs. *The Annals of Statistics*, 48(1):539–559, 2020.

S. W. Mogensen and N. R. Hansen. Graphical modeling of stochastic processes driven by correlated noise. *Bernoulli*, 28(4):3023–3050, 2022.

V. Nenna, A. Pidlisecky, and R. Knight. Application of an extended kalman filter approach to inversion of time-lapse electrical resistivity imaging data for monitoring recharge. *Water Resources Research*, 47(10), 2011.

J. N. Nielsen, H. Madsen, and P. C. Young. Parameter estimation in stochastic differential equations: an overview. *Annual Reviews in Control*, 24:83–94, 2000.

M. Nutz. Introduction to entropic optimal transport. *Lecture notes, Columbia University*, 2021.

D. R. O’Connor et al. Part two: Report of the walkerton inquiry: A strategy for safe drinking water. Technical report, Ministry of the Attorney General, 2002.

W. Ogle et al. *Aristotle: on the parts of animals*. Kegan Paul, French & Company, 1882.

J. Oh and C. W. Tsai. A stochastic jump diffusion particle-tracking model (sjd-ptm) for sediment transport in open channel flows. *Water Resources Research*, 46(10), 2010.

B. Oksendal. *Stochastic differential equations: an introduction with applications*. Springer Science & Business Media, 2013.

A. J. Paulson. The transport and fate of fe, mn, cu, zn, cd, pb and so4 in a groundwater plume and in downstream surface waters in the coeur d’alene mining district, idaho, usa. *Applied Geochemistry*, 12(4):447–464, 1997.

G. A. Pavliotis. Stochastic processes and applications. *Texts in Applied Mathematics*, 60, 2014.

R. Pawlowicz, C. Hannah, and A. Rosenberger. Lagrangian observations of estuarine residence times, dispersion, and trapping in the salish sea. *Estuarine, Coastal and Shelf Science*, 225: 106246, 2019.

S. Peiris, R. Mellor, and P. Ainkaran. Maximum likelihood estimation for short time series with replicated observations: A simulation study. *InterStat*, 9:1–16, 2003.

K. B. Petersen, M. S. Pedersen, et al. The matrix cookbook. *Technical University of Denmark*, 7 (15):510, 2008.

G. Peyré, M. Cuturi, et al. Computational optimal transport: With applications to data science. *Foundations and Trends® in Machine Learning*, 11(5-6):355–607, 2019.

A. Reisach, C. Seiler, and S. Weichwald. Beware of the simulated dag! causal discovery benchmarks may be easy to game. *Advances in Neural Information Processing Systems*, 34:27772–27784, 2021.

M. Rohbeck, B. Clarke, K. Mikulik, A. Pettet, O. Stegle, and K. Ueltzhöffer. Bicycle: Intervention-based causal discovery with cycles. In *Causal Learning and Reasoning*, pages 209–242. PMLR, 2024.

J. Runge. Necessary and sufficient graphical conditions for optimal adjustment sets in causal graphical models with hidden variables. *Advances in Neural Information Processing Systems*, 34:15762–15773, 2021.

P. Salamon, D. Fernàndez-Garcia, and J. Gómez-Hernández. Modeling tracer transport at the made site: The importance of heterogeneity. *Water Resources Research*, 43(8), 2007.

A. Santos, D. Rente, R. Seabra, and J. M. Moura. Learning the causal structure of networked dynamical systems under latent nodes and structured noise. In *Proceedings of the AAAI Conference on Artificial Intelligence*, volume 38, pages 14866–14874, 2024.

S. Särkkä and A. Solin. *Applied stochastic differential equations*, volume 10. Cambridge University Press, 2019.

G. Schiebinger, J. Shu, M. Tabaka, B. Cleary, V. Subramanian, A. Solomon, J. Gould, S. Liu, S. Lin, P. Berube, et al. Optimal-transport analysis of single-cell gene expression identifies developmental trajectories in reprogramming. *Cell*, 176(4):928–943, 2019.

M. Setty, M. D. Tadmor, S. Reich-Zeliger, O. Angel, T. M. Salame, P. Kathail, K. Choi, S. Bendall, N. Friedman, and D. Pe'er. Wishbone identifies bifurcating developmental trajectories from single-cell data. *Nature biotechnology*, 34(6):637–645, 2016.

Y. Shen, R. Berlinghieri, and T. Broderick. Learning a vector field from snapshots of unidentified particles rather than particle trajectories. In *ICLR 2024 Workshop on AI4DifferentialEquations In Science*, 2024a.

Y. Shen, R. Berlinghieri, and T. Broderick. Multi-marginal schrödinger bridges with iterative reference. *arXiv preprint arXiv:2408.06277*, 2024b.

Y. Shi, V. De Bortoli, A. Campbell, and A. Doucet. Diffusion schrödinger bridge matching. *Advances in Neural Information Processing Systems*, 36, 2024.

D. W. Stroock. *Partial differential equations for probabalists [sic]*. Cambridge University Press, 2008.

A. Tejada-Lapuerta, P. Bertin, S. Bauer, H. Aliee, Y. Bengio, and F. J. Theis. Causal machine learning for single-cell genomics. *arXiv preprint arXiv:2310.14935*, 2023.

A. Terpin, N. Lanzetti, and F. Dörfler. Learning diffusion at lightspeed. *arXiv preprint arXiv:2406.12616*, 2024.

C. Trapnell, D. Cacchiarelli, J. Grimsby, P. Pokharel, S. Li, M. Morse, N. J. Lennon, K. J. Livak, T. S. Mikkelsen, and J. L. Rinn. The dynamics and regulators of cell fate decisions are revealed by pseudotemporal ordering of single cells. *Nature biotechnology*, 32(4):381–386, 2014.

F. Vargas, P. Thodoroff, A. Lamacraft, and N. Lawrence. Solving schrödinger bridges via maximum likelihood. *Entropy*, 23(9):1134, 2021.

C. Waddington. How animal develop, 1935.

Y. Wang, X. Geng, W. Huang, B. Huang, and M. Gong. Generator identification for linear sdes with additive and multiplicative noise. *Advances in Neural Information Processing Systems*, 36, 2024.

C. Weinreb, S. Wolock, B. K. Tusi, M. Socolovsky, and A. M. Klein. Fundamental limits on dynamic inference from single-cell snapshots. *Proceedings of the National Academy of Sciences*, 115(10): E2467–E2476, 2018.

H. White. Maximum likelihood estimation of misspecified models. *Econometrica: Journal of the econometric society*, pages 1–25, 1982.

R. E. Williamson and H. F. Trotter. Multivariable mathematics: linear algebra, differential equations, calculus. *(No Title)*, 1974.

T. Yachimura, H. Wang, Y. Imoto, M. Yoshida, S. Tasaki, Y. Kojima, Y. Yabuta, M. Saitou, and Y. Hiraoka. scegot: Single-cell trajectory inference framework based on entropic gaussian mixture optimal transport. *bioRxiv*, pages 2023–09, 2023.

S. Y. Zhang. Joint trajectory and network inference via reference fitting. *arXiv preprint arXiv:2409.06879*, 2024.

W. Zhao, E. Larschan, B. Sandstede, and R. Singh. Optimal transport reveals dynamic gene regulatory networks via gene velocity estimation. *bioRxiv*, pages 2024–09, 2024.